PERGAMON

International Journal of Solids and Structures 39 (2002) 2153–2188

INTERNATIONAL JOURNAL OF SOLIDS and STRUCTURES

www.elsevier.com/locate/ijsolstr

Homogenized elastic properties of honeycomb sandwich with skin effect

X. Frank Xu [a,b], Pizhong Qiao [a,*]

[a] *Department of Civil Engineering, The University of Akron, Akron, OH 44325-3905, USA*
[b] *Department of Civil Engineering, The Johns Hopkins University, Baltimore, MD 21218, USA*

Received 19 July 2001; received in revised form 27 December 2001

Abstract

The adaptation of homogenization theory to periodic plates is presented and extended to include transverse shear deformation theory for a honeycomb sandwich. Based on the scaling asymptotic expansions about plate thickness δ for sandwiches with comparable characteristic periodicity ε, the homogenization functions Π, U, and V are formulated implicitly in 3-D elliptical equations corresponding to the modes of transverse shear, in-plane stretch and out-plane bending. The solutions of these periodic functions are analytically obtained through a multi-pass homogenization technique that includes the first pass of a geometry-to-material transformation model and the second pass of 2-D unit cell homogenization. The derivation not only leads to analytical formulas of homogenized (To distinguish the homogenization between micro-scale and meso-scale, the term 'homogenized' or 'equivalent' is hereby used in meso-scale, corresponding to the term 'effective' for micro-scale.) elastic stiffness of honeycomb sandwiches, but also demonstrates the significance of usually neglected skin effect on honeycomb computations. Finally, a periodic unit cell finite element modeling technique is developed to validate the analytical approach and further complement it with skin rigidity considered.

Keywords: Honeycomb sandwiches; Homogenization; Plate theory; Cellular structures; Equivalent stiffness; Skin effect; Multi-pass homogenization; Geometry-to-material transformation model; Unit cell finite element modeling

1. Introduction

A typical honeycomb sandwich panel consists of two thin and stiff facing materials bonded to a thick and lightweight thin-walled core with in-plane two-dimension periodic cellular structure. The characteristic of three-layer arrangement, intuitively, leads to classical sandwich theory (e.g., Allen, 1969; Plantema, 1966; Zenkert, 1995), a beginning and a branch of present laminate theory. The computational models on honeycomb sandwiches, as reviewed by Noor et al. (1996), are generally based on the equivalent replacement of honeycomb cores with homogeneous continuum due to expensive computations of 3-D detailed finite element analysis (FEA). Obviously the reliability of continuum modeling is critically dependent

* Corresponding author. Tel.: +1-330-972-5226; fax: +1-330-972-6020.
E-mail address: qiao@uakron.edu (P. Qiao).

0020-7683/02/$ - see front matter
PII: S0020-7683(02)00111-7

on the accuracy of equivalent core properties. And today the concern is further strengthened by research interests on more detailed local fields such as impact delamination, dynamic failure, and various local buckling modes. The application of laminate theory on meso-cell honeycomb sandwich panels, however, has been found not so successful as on micro-cell composite laminates. The difficulty is first encountered by the acquisition of homogenized properties of honeycomb sandwiches, as so far the discussions have still been open on 3-D derivations and, no less importantly, on how to fit them into the frameworks of existing computational models. One common example is the appropriate determination of mechanical properties for brick elements as core equivalence in the static, dynamic and thermal FEA of sandwich panels, which remains a problem in honeycomb continuum modeling, e.g., as assessed by Burton and Noor (1997).

Conventional hexagonal honeycomb sandwiches have been widely applied in aerospace industry since 1940s. With the development of composite materials and manufacturing technology, the application of this efficient structure has been penetrating into every possible field. Circumstantially honeycomb sandwiches can be optimized from geometry to material in both global and local levels. Among them, one important choice is of honeycomb cores, where the size, shape, topology and wall thickness of core configuration and constituent materials can be comprehensively optimized by taking account of local interactions and consequent global behaviors.

The natural efficiency of cellular structures has thus attracted many investigations (e.g., Gibson and Ashby, 1988; Warren and Kraynik, 1987; Fortes and Ashby, 1999) on periodic and disordered cells, wherein the book of Gibson and Ashby (1988) is the first systematic literature in the field. Of the fundamental equivalent elastic properties, the in-plane elastic properties of honeycomb were first obtained with the standard beam theory (Gibson and Ashby, 1988; Masters and Evans, 1996). Further refinements, e.g., as introduced by Masters and Evans (1996), have been attempted considering stretching and hinging effects and the extension to finer scale of molecular modeling. It must be pointed out that all these mathematical models on honeycomb cores are built based on pure cellular structures, and the usual presence of strengthening skin faces has not been taken into account. In classical sandwich theory (Allen, 1969), the global skin–core interaction is identified as the result of the anti-plane core assumption. Since the constraints of two skin faces significantly alter local deformation mechanism of a heterogeneous core, the homogenized core stiffness properties become sensitive to the ratio of core thickness to unit cell size, which is called skin effect in this paper or thickness effect by Becker (1998). The practice of neglecting skin effect is prevalent in today's sandwich research and design, wherein the equivalent core properties are simply taken from those formulas based on pure cellular models. Besides other unscrupulous uses causing erroneous Poisson's ratios and singularities, this neglect yields underestimate of stiffness and subsequent inconsistencies between modeling and reality, although only few of them were noticed in experiments (e.g., the study by Cunningham and White, 2001). A common example is the anti-plane core assumption in sandwich beam analysis, where skin effect and edge effect of anti-clastic bending have been too simply ignored. As observed in experiments (e.g., Adams and Maheri, 1993; Daniel and Abot, 2000), skin constraints were demonstrated by the phenomenon of skin lateral contraction and expansion.

The skin effect, induced by high gradient of material change between two skin faces and a heterogeneous core, can be analogous to heterogeneous multi-phase interactions in micromechanics of composites. The homogenization theory, well applied in 3-D micro-scale periodic composite materials, has been adapted into heterogeneous plate and shell theory since the 1970s (Duvaut, 1977; Caillerie, 1984). The theoretical efforts made in obtaining plate equivalent properties are highly dependent on the simplifications given by the constraint assumptions of a corresponding plate theory, i.e., Kirchhoff, Reissner–Hencky or Reddy plate theories (Lewinski, 1991). And the approximations are processed based on the ratio of plate's two small parameters, i.e., characteristic thickness δ and characteristic periodicity ε. When $\delta/\varepsilon \sim 0$, such as lattice plate, the plate assumption of unit cell results in simple analytical formulas (Lewinski, 1991; Caillerie, 1984). When $\delta/\varepsilon \gg 1$, as in the case of fiber composite laminates, the equivalent stiffness properties of laminates are derived from the micromechanics between fiber and matrix in each individual sub-

layers, such as classical laminate plate theory (CLPT) resulting from the plane stress assumption. In the case of $\delta/\varepsilon \sim 1$, the asymptotic expansion method or Γ-convergence technique generates the Caillerie–Kohn–Vogelius plate model, which is difficult to apply analytically (Lewinski, 1991). Hence honeycomb sandwiches, fallen into the domain of $\delta/\varepsilon \sim 1$, have been conventionally treated by laminate theory, where a honeycomb core is firstly homogenized into a continuum equivalent layer separately, and then the skin–core interactions are modeled with CLPT or higher order laminate theories. Clearly even with higher order terms, the conventional approach fails to realize the heterogeneity of cores and the consequent high gradient of through-thickness mechanical variables.

In conventional sandwich analysis, the three-layer sandwich theory requires equivalent properties of a pure core, which should be accountable for real skin–core interactions in both global and local sense, i.e., the interactions must be energetically equivalent prior to and posterior to the homogenization of the core. There have been many refined theories and finite elements proposed to overcome the complicated interaction problem. In this paper, a straightforward approach is proposed to homogenize a unit cell including both skin faces and core, by which skin effect can not only be accounted for locally but also be assessed precisely. A homogenized single-layer plate model then can be constructed with the properties derived based on shear deformable plate theory. Further, with this approach the sandwich local behaviors can be accurately predicted by using inverse or unsmearing procedure, which is expected as an important advantage over any conventional refined theories. One example is of the local stability problem, where the critical wrinkling load is strongly dependent on the in-plane stiffness (Vonach and Rammerstorfer, 1998). The diagram of comparison between conventional and proposed approaches is shown in Figs. 1 and 2.

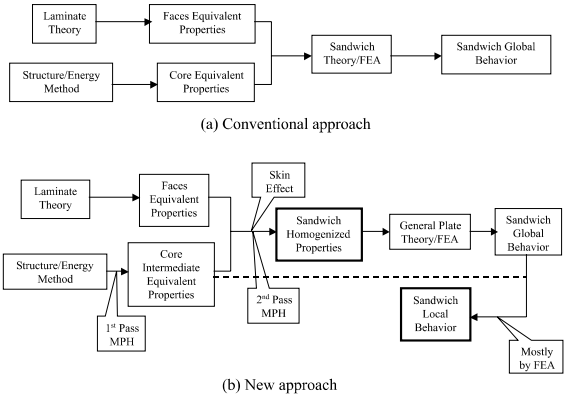

Fig. 1. Diagram of two approaches for honeycomb sandwich analysis. (a) Conventional approach and (b) new approach.

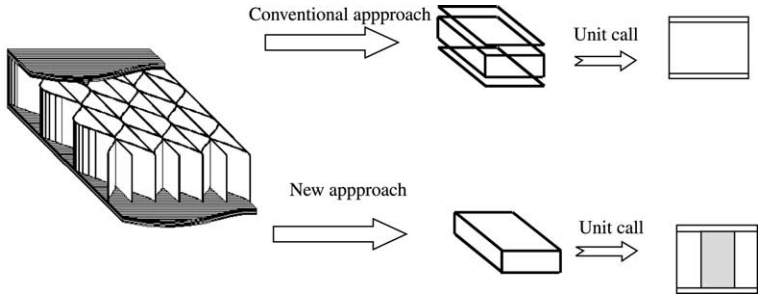

Fig. 2. Comparison of two approaches for honeycomb sandwich analysis.

2. Literature review

The phenomenon of honeycomb skin effect was first assessed by Kelsey et al. (1958), and the equivalent transverse shear stiffness of hexagonal honeycomb core was investigated. The skin effect on the transverse shear deformation was theoretically expressed by two bounds of derived equivalent shear stiffness, whereas the lower and upper bounds correspond to zero and infinite large skin effect, respectively. Later Penzien and Didriksson (1964) improved Kelsey's upper bound (UB) by formulating a closer displacement field than Kelsey's uniform field, and the solution consistently showed the trend of the diminishing skin effect with the increase of core thickness ratio δ/ε. More recently, Shi and Tong (1995a) applied 2-D homogenization technique to obtain Kelsey's lower bound (LB) value, and Xu et al. (2001) extended it to general honeycomb configurations. Numerical approaches on transverse shear stiffness were attempted by Shi and Tong (1995a) and Grediac (1993). Shi and Tong (1995a) used a specialized hybrid element; however the results are found neither consistent with Penzien and Didriksson's (1964) conclusion nor with Saint–Venant theorem explained by Grediac (1993). In the study by Grediac (1993), the applied unit cell boundary conditions actually correspond to those of the analytical approximations of Penzien and Didriksson (1964); thus the results only numerically verify latter's work without providing better accuracies.

Unlike the evaluations of equivalent shear stiffness of honeycomb cores, the skin effect on other stiffness tensors has received less attention. Both Parton and Kudryavtsev (1993) and Shi and Tong (1995b) solved the honeycomb equivalent in-plane stiffness by two-scale method; however, the skin effect was not considered in their studies. Through an energy minimization implementation, Becker (1998) for the first time assessed the skin effect on equivalent in-plane moduli. A further expansion was attempted recently by Hohe and Becker (2001) to include all elastic tensors and general honeycomb cores with but quite implicit lengthy calculations. For a sandwich panel, the very important concern is the flexural stiffness contributed from a honeycomb core. Among few existing references, only Parton and Kudryavtsev (1993) gave a formula for flexural stiffness of honeycomb cores, which is simply derived from in-plane stretch stiffness and does not include skin effect. In this paper, to the authors' knowledge, flexural stiffness is first time distinguished from stretch stiffness, since the displacement field varies when loading is changed from symmetry to antisymmetry about the panel middle plane.

There are several engineering investigations (Chamis et al., 1988; Takano et al., 1995; Bourgeois et al., 1998; Vougiouka and Guedes, 1998; Meraghni et al., 1999) on the homogenization of honeycomb sandwiches; however they are case limited without further insight. Besides addressing the aforementioned unsolved issues, this paper is aimed to develop an effective approach to homogenize general honeycomb cells and to provide a comprehensive approach in three aspects—the mathematical statement of sandwich homogenization theory, analytical solution of a multi-pass homogenization (MPH) technique, and a 3-D unit cell FEA homogenization technique.

The MPH technique originates from the conception that the homogenization of an object can be processed by its principal axes one by one, i.e., the homogenized results obtained along one axis can be well applied to the next pass along another axis. In this paper, the MPH technique includes a two-pass procedure to homogenize 3-D geometrical heterogeneous honeycomb media in orthogonal directions. The first pass involves the building of a geometry-to-material transformation model (GTM), by which the complicated 3-D spatial analysis is simplified into a 2-D plane stress or plane strain case. The first pass, i.e., the GTM, is mathematically equivalent to the coordinates transformation in combination with energetic averaging. The coordinates transformation has been conventionally applied by all the relevant research referenced in this paper, and the process however is inconvenient and lengthy. The MPH technique and sandwich homogenization formulation developed here can efficiently simplify the process and be applicable for all general sandwich structures with periodic cores. In the second pass, with the resulting intermediate core equivalent properties, the appropriate displacement field is constructed by satisfying field equations either exactly or weakly. With the homogenization formulation given in Section 3, or with energy mini-

mization theorem, the homogenized stiffness can be analytically solved in the form of Fourier series. In Section 5, the FEA numerical results verify the semi-analytical solutions, which further complementally show the influence of skin rigidity. A specialized FE modeling technique is developed at the end of this paper for the appropriate imposing of periodic boundary conditions in unit cell FEA modeling. This technique can be easily used in commercial FEA programs without writing specialized code for hybrid elements, and the principle of which is extendable to all periodic media of unit cell FEA.

3. Formulation of honeycomb homogenization problem

3.1. Asymptotic expansions about plate thickness δ

The asymptotic expansion for plates with $\delta/\varepsilon \sim 1$ was first given by Caillerie (1984). Hereby the expansion is repeated, and the notations are made consistent with the derivation of Kirchhoff–Love plate model by Parton and Kudryavtsev (1993), where small Latin indices denote 1, 2, 3 and small Greek indices for 1, 2. To extend the homogenized plate model to transverse shear deformation theory, the formulation of homogenized transverse shear stiffness is attempted in Section 3.2.

For common honeycomb sandwiches (see Fig. 3) of which the body force is ignored, the 3-D elasticity field equations and boundary conditions can be written as

$$\begin{aligned} &\frac{\partial \sigma_{ij}}{\partial x_j} = 0, \quad \text{in } \Omega \\ &u_i = \widehat{u_i}, \quad \text{on } \partial_1\Omega \\ &\sigma_{ij} n_j = T_i, \quad \text{on } \partial_2\Omega \end{aligned} \tag{1}$$

where

$$\begin{aligned} &\sigma_{ij} = c_{ijkl} e_{kl} \\ &e_{kl} = \frac{1}{2}\left(\frac{\partial u_k}{\partial x_l} + \frac{\partial u_l}{\partial x_k}\right) \end{aligned} \tag{2}$$

And the coefficient c_{ijkl} should satisfy the elliptical symmetry condition

$$c_{ijkl} = c_{jikl} = c_{ijlk} = c_{klij}$$

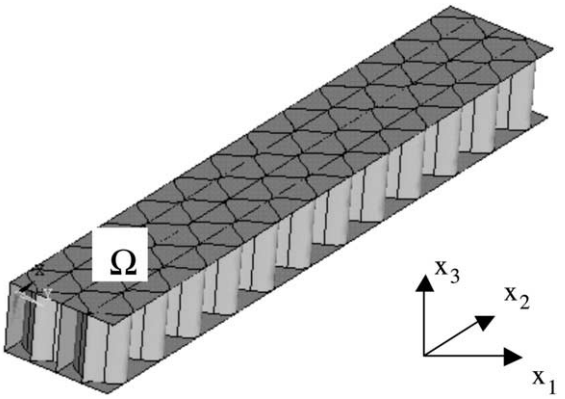

Fig. 3. A body of honeycomb sandwich structure.

A dimensionless small parameter, δ, characterizes the ratio of the plate thickness to the plate global size, L, and hereby the local coordinates of the unit cell are introduced to rescale the problem

$$y_1 = \frac{x_1}{h_1\delta} \qquad y_2 = \frac{x_2}{h_2\delta} \qquad z = \frac{x_3}{\delta} \tag{3}$$

where $\boldsymbol{h}$ characterizes the ratio of the unit cell size to the plate thickness which ensures the rescaled unit cell domain in $\{-1/2 < y_1, y_2, z < 1/2\}$.

With the two-scale expansion method about the small parameter δ, the series are expressed as

$$\begin{aligned} u_i^{(\varepsilon)} &= u_i^{(0)}(x) + \delta u_i^{(1)}(x,y,z) + \cdots \\ e_{ij}^{(\varepsilon)} &= e_{ij}^{(0)}(x,y,z) + \delta e_{ij}^{(1)}(x,y,z) + \cdots \\ \sigma_{ij}^{(\varepsilon)} &= \sigma_{ij}^{(0)}(x,y,z) + \delta \sigma_{ij}^{(1)}(x,y,z) + \cdots \end{aligned} \tag{4}$$

where the strain–displacement law is

$$\begin{aligned} e_{\alpha\beta}^{(l)} &= \varepsilon_{\alpha\beta}^{(l)} + \frac{1}{2}\left(\frac{1}{h_\beta}\frac{\partial u_\alpha^{(l+1)}}{\partial y_\beta} + \frac{1}{h_\alpha}\frac{\partial u_\beta^{(l+1)}}{\partial y_\alpha}\right) \\ e_{\alpha 3}^{(l)} &= \frac{1}{2}\varepsilon_{\alpha 3}^{(l)} + \frac{1}{2}\left(\frac{\partial u_\alpha^{(l+1)}}{\partial z} + \frac{1}{h_\alpha}\frac{\partial u_3^{(l+1)}}{\partial y_\alpha}\right) \\ e_{33}^{(l)} &= \frac{\partial u_3^{(l+1)}}{\partial z} \\ \varepsilon_{\alpha\beta}^{(l)} &= \frac{1}{2}\left(\frac{\partial u_\alpha^{(l)}}{\partial x_\beta} + \frac{\partial u_\beta^{(l)}}{\partial x_\alpha}\right) \\ \varepsilon_{\alpha 3}^{(l)} &= \frac{\partial u_3^{(l)}}{\partial x_\alpha} \\ l &= 0, 1, 2, \ldots \end{aligned} \tag{5}$$

and the constitutive equations are

$$\sigma_{ij}^{(l)} = c_{ijkl} e_{kl}^{(l)} \quad l = 0, 1, 2, \ldots \tag{6}$$

The external traction T is assumed only being applied in the transverse direction, which can be written as function of δ by

$$T_3^{\pm z}(x) = \delta^3 q^{\pm z}(x,y) \tag{7}$$

By matching the expansion terms, the boundary traction conditions are known

$$\begin{aligned} &\sigma_{i3}^{(l)}\Big|_{z=\pm\frac{1}{2}} = 0, \quad l = 0, 1, 2 \\ &\sigma_{13}^{(3)}\Big|_{z=\pm\frac{1}{2}} = \sigma_{23}^{(3)}\Big|_{z=\pm\frac{1}{2}} = 0, \qquad \sigma_{33}^{(3)}\Big|_{z=\pm\frac{1}{2}} = q^{\pm z}(x,y) \end{aligned} \tag{8}$$

Note the variables with superscript $l > 0$ are all Y-periodic in y. Substituting (4)–(6) into (1) and matching the power order of δ result

$$\begin{aligned}
&\frac{1}{h_\alpha}\frac{\partial \sigma_{i\alpha}^{(0)}}{\partial y_\alpha}+\frac{\partial \sigma_{i3}^{(0)}}{\partial z}=0\\
&\frac{\partial \sigma_{i\alpha}^{(l)}}{\partial x_\alpha}+\frac{1}{h_\alpha}\frac{\partial \sigma_{i\alpha}^{(l+1)}}{\partial y_\alpha}+\frac{\partial \sigma_{i3}^{(l+1)}}{\partial z}=0, \quad l=0,1,2,\ldots
\end{aligned} \tag{9}$$

With the substitution of (4)–(6) into (9) and the consideration of the boundary conditions in (8), the following can be derived as detailed by Parton and Kudryavtsev (1993)

$$\begin{aligned}
&u_\alpha^{(0)}=0\\
&u_3^{(0)}(x)=w(x)\\
&u_\alpha^{(1)}=v_\alpha^{(1)}-z\frac{\partial w}{\partial x_\alpha}\\
&\sigma_{ij}^{(0)}=0
\end{aligned} \tag{10}$$

from which the displacements can be expressed by global in-plane and flexural variables as

$$\begin{aligned}
u_\alpha^{(\varepsilon)}&=\delta v_\alpha^{(1)}(x)-x_3\frac{\partial w}{\partial x_\alpha}+\delta^2 U_\alpha^{\mu\nu}\varepsilon_{\mu\nu}^{(1)}+\delta^2 V_\alpha^{\mu\nu}\kappa_{\mu\nu}^{(0)}+\cdots\\
u_3^{(\varepsilon)}&=w(x)+\delta^2\tilde{u}_3^{(2)}(x)+\delta^2 U_3^{\mu\nu}\varepsilon_{\mu\nu}^{(1)}+\delta^2 V_3^{\mu\nu}\kappa_{\mu\nu}^{(0)}+\cdots
\end{aligned} \tag{11}$$

where

$$\begin{aligned}
&\kappa_{\mu\nu}^{(0)}=-\frac{\partial^2 w}{\partial x_\mu \partial x_\nu}\\
&\varepsilon_{\mu\nu}^{(1)}=\frac{1}{2}\left(\frac{\partial v_\mu^{(1)}}{\partial x_\nu}+\frac{\partial v_\nu^{(1)}}{\partial x_\mu}\right)
\end{aligned} \tag{12}$$

Note in Parton and Kudryavtsev (1993), the transverse shear deformation is ignored, whilst in this paper the additional term $\delta^2\tilde{u}_3^{(2)}(x)$ in (11) is obtained by modification of equation (19.51) of Parton and Kudryavtsev (1993) as follows:

$$u_3^{(2)}(x,y,z)=U_3^{\mu\nu}\varepsilon_{\mu\nu}^{(1)}+V_3^{\mu\nu}\kappa_{\mu\nu}^{(0)}+\tilde{u}_3^{(2)}(x) \tag{13}$$

In the above equations, the commonly called homogenization functions $U(y,z)$ and $V(y,z)$ are the local periodic displacements induced by in-plane strain $\varepsilon_{\mu\nu}^{(1)}$ and flexural curvature $\kappa_{\mu\nu}^{(0)}$, respectively, which should satisfy the local equilibrium equations

$$\begin{aligned}
&\langle\sigma_{\mu\nu}^{(1)}\rangle=\langle C_{\mu\nu\alpha\beta}\rangle\varepsilon_{\alpha\beta}^{(1)}+\langle C_{\mu\nu\alpha\beta}^{*}\rangle\kappa_{\alpha\beta}^{(0)}\\
&\langle z\sigma_{\mu\nu}^{(1)}\rangle=\langle zC_{\mu\nu\alpha\beta}\rangle\varepsilon_{\alpha\beta}^{(1)}+\langle zC_{\mu\nu\alpha\beta}^{*}\rangle\kappa_{\alpha\beta}^{(0)}
\end{aligned} \tag{14}$$

$$\begin{aligned}
C_{\mu\nu\alpha\beta}&=c_{\mu\nu\alpha\beta}+c_{\mu\nu i\lambda}\frac{1}{h_\lambda}\frac{\partial U_i^{\alpha\beta}}{\partial y_\lambda}+c_{\mu\nu i3}\frac{\partial U_i^{\alpha\beta}}{\partial z}\\
C_{\mu\nu\alpha\beta}^{*}&=zc_{\mu\nu\alpha\beta}+c_{\mu\nu i\lambda}\frac{1}{h_\lambda}\frac{\partial V_i^{\alpha\beta}}{\partial y_\lambda}+c_{\mu\nu i3}\frac{\partial V_i^{\alpha\beta}}{\partial z}
\end{aligned} \tag{15}$$

and uniqueness conditions

$$\begin{aligned} &\langle U_i^{\alpha\beta}\rangle_y = 0, \quad \text{at } z = 0 \\ &\langle V_i^{\alpha\beta}\rangle_y = 0, \quad \text{at } z = 0 \end{aligned} \tag{16}$$

we henceforth denote averaging operators $\langle\times\rangle = \int_{\Omega_p} \times \,\mathrm{d}y_1\,\mathrm{d}y_2\,\mathrm{d}z, \qquad \langle\times\rangle_y = \int_Y \times \,\mathrm{d}y_1\,\mathrm{d}y_2$

3.2. Homogenized transverse shear plate model

To take into account the transverse shear deformation, instead of (16), the uniqueness conditions are redefined as

$$\begin{aligned} &\langle c_{\alpha 3\beta 3} U_3^{\alpha\beta}\rangle = 0 \\ &\langle c_{\alpha 3\beta 3} V_3^{\alpha\beta}\rangle = 0 \end{aligned} \tag{17}$$

By applying the averaging process to (9) for $l = 2$ with Green–Gauss theorem, it gives

$$\frac{\partial\langle\sigma_{3\alpha}^{(2)}\rangle}{\partial x_\alpha} + q(x) = 0 \tag{18}$$

$$q(x) = \int_Y q^{\pm z}(x,y)\,\mathrm{d}y \tag{19}$$

Assume material properties are monoclinic in that $c_{\alpha\beta\mu 3} = c_{\alpha 333} = 0$. Using (5) and (6), we have

$$\sigma_{3\alpha}^{(2)} = c_{3\alpha 3\beta}\left(\frac{\partial u_3^{(2)}(x,y,z)}{\partial x_\beta} + \frac{\partial u_\beta^{(3)}}{\partial z} + \frac{1}{h_\beta}\frac{\partial u_3^{(3)}}{\partial y_\beta}\right) \tag{20}$$

Let

$$\begin{aligned} &\gamma_{3\beta}^{(2)} = \frac{\partial \tilde{\boldsymbol{u}}_3^{(2)}(x)}{\partial x_\beta} \\ &u_i^{(3)} = \Pi_i^\beta \gamma_{3\beta}^{(2)} \end{aligned} \tag{21}$$

where Π is the local periodic displacement function induced by the transverse shear. Define equivalent transverse shear stiffness $\langle C_{\alpha 3\beta 3}\rangle$ by

$$\langle\sigma_{3\alpha}^{(2)}\rangle = \langle C_{\alpha 3\beta 3}\rangle\gamma_{3\beta}^{(2)} \tag{22}$$

Then by (13), (17), (20)–(22) and for $\varepsilon_{\mu\nu}^{(1)}$ even about z, $C_{\alpha 3\beta 3}$ can be written as

$$C_{\alpha 3\beta 3} = c_{\alpha 3\beta 3} + c_{\alpha 3\lambda 3}\left(\frac{\partial \Pi_\lambda^\beta}{\partial z} + \frac{1}{h_\lambda}\frac{\partial \Pi_3^\beta}{\partial y_\lambda}\right) \tag{23}$$

Thus (15) and (22) give all the stiffness required for transverse shear deformation theory of plates. And the stress and moment resultants can be written as

$$\begin{aligned} N_{\alpha\beta} &= \delta^2\langle C_{\alpha\beta\mu\nu}\rangle\varepsilon_{\mu\nu}^{(1)} + \delta^2\langle C_{\alpha\beta\mu\nu}^*\rangle\kappa_{\mu\nu}^{(0)} \\ M_{\alpha\beta} &= \delta^3\langle z C_{\alpha\beta\mu\nu}\rangle\varepsilon_{\mu\nu}^{(1)} + \delta^3\langle z C_{\alpha\beta\mu\nu}^*\rangle\kappa_{\mu\nu}^{(0)} \\ Q_\alpha &= \delta^3\langle C_{\alpha 3\beta 3}\rangle\gamma_{3\beta}^{(2)} \end{aligned} \tag{24}$$

For transversely symmetric honeycomb sandwiches, clearly in-plane and flexural couple disappears, i.e., $\langle zC_{\alpha\beta\mu\nu}\rangle = \langle C^*_{\alpha\beta\mu\nu}\rangle = 0$. From (11), the global strain variables are correspondingly given by

$$\begin{aligned}\gamma_{3\beta} &= \delta^2\gamma^{(2)}_{3\beta}\\ \varepsilon_{\mu\nu} &= \delta\varepsilon^{(1)}_{\mu\nu}\\ \kappa_{\mu\nu} &= \kappa^{(0)}_{\mu\nu}\end{aligned} \tag{25}$$

Further for symbolic consistence with CLPT and by (24) and (25), the plate macroscopic equivalent stiffness may be finally expressed as

$$\begin{aligned}N_{\alpha\beta} &= A^H_{\alpha\beta\mu\nu}\varepsilon_{\mu\nu}, \qquad A^H_{\alpha\beta\mu\nu} = \delta\langle C_{\alpha\beta\mu\nu}\rangle\\ M_{\alpha\beta} &= D^H_{\alpha\beta\mu\nu}\kappa_{\mu\nu}, \qquad D^H_{\alpha\beta\mu\nu} = \delta^3\langle zC^*_{\alpha\beta\mu\nu}\rangle\\ Q_\alpha &= H^H_{\alpha3\beta3}\gamma_{3\beta}, \qquad H^H_{\alpha3\beta3} = \delta\langle C_{\alpha3\beta3}\rangle\end{aligned} \tag{26}$$

or more clearly for sandwich panels with three planes of symmetry

$$\begin{bmatrix}N_{11}\\ N_{22}\\ N_{66}\end{bmatrix} = \begin{bmatrix}A_{11} & A_{12} & 0\\ A_{21} & A_{22} & 0\\ 0 & 0 & A_{66}\end{bmatrix}\begin{bmatrix}\varepsilon_{11}\\ \varepsilon_{22}\\ \varepsilon_{66}\end{bmatrix}$$
$$\begin{bmatrix}M_{11}\\ M_{22}\\ M_{66}\end{bmatrix} = \begin{bmatrix}D_{11} & D_{12} & 0\\ D_{21} & D_{22} & 0\\ 0 & 0 & D_{66}\end{bmatrix}\begin{bmatrix}\kappa_{11}\\ \kappa_{22}\\ \kappa_{66}\end{bmatrix}, \qquad \begin{bmatrix}Q_{44}\\ Q_{55}\end{bmatrix} = \begin{bmatrix}H_{44} & 0\\ 0 & H_{55}\end{bmatrix}\begin{bmatrix}\gamma_{44}\\ \gamma_{55}\end{bmatrix} \tag{27}$$

where contracted notation is introduced with $\alpha\alpha\beta\beta = \alpha\beta$, $2323 = 3232 = 44$, $1313 = 3131 = 55$, and $1212 = 2121 = 66$.

3.3. Field equations of three local problems

From (15) and (23), the homogenized stiffness can be obtained once the solutions of the homogenization functions $U(y,z)$, $V(y,z)$ and $\Pi(y,z)$ are known. These periodic functions then have to be solved by the local elastic equilibrium equations as given in (9), combined with unit cell periodic boundary conditions. It should be noted that in all the following equations, the material properties $[c]$ are function of spatial coordinate, and assumed monoclinic in that $c_{\alpha\beta\mu3} = c_{\alpha333} = 0$.

3.3.1. Transverse shear local problem $\Pi(y,z)$

Assume a pure shear case that $\varepsilon = \kappa = 0$. Combining (9), (20) and (21), the equilibrium equations become

$$\begin{aligned}&\frac{1}{h_\alpha}\frac{\partial}{\partial y_\alpha}\left[c_{\alpha3\beta3} + c_{\alpha3\mu3}\left(\frac{\partial\Pi^\beta_\mu}{\partial z} + \frac{1}{h_\mu}\frac{\partial\Pi^\beta_3}{\partial y_\mu}\right)\right] + \frac{\partial}{\partial z}\left(c_{33\nu\lambda}\frac{1}{h_\lambda}\frac{\partial\Pi^\beta_\nu}{\partial y_\lambda} + c_{3333}\frac{\partial\Pi^\beta_3}{\partial z}\right) = 0\\ &\frac{1}{h_\mu}\frac{\partial}{\partial y_\mu}\left(c_{\alpha\mu33}\frac{\partial\Pi^\beta_3}{\partial z} + c_{\alpha\mu\nu\nu}\frac{1}{h_\nu}\frac{\partial\Pi^\beta_\nu}{\partial y_\nu}\right) + \frac{\partial}{\partial z}\left[c_{\alpha3\beta3} + c_{\alpha3\lambda3}\left(\frac{\partial\Pi^\beta_\lambda}{\partial z} + \frac{1}{h_\lambda}\frac{\partial\Pi^\beta_3}{\partial y_\lambda}\right)\right] = 0\end{aligned} \tag{28}$$

From (5), the boundary conditions are specified as

$$\begin{aligned}&c_{33\nu\lambda}\frac{1}{h_\lambda}\frac{\partial\Pi^\beta_\nu}{\partial y_\lambda} + c_{3333}\frac{\partial\Pi^\beta_3}{\partial z} = 0 \qquad z = z^\pm\\ &c_{\alpha3\beta3} + c_{\alpha3\lambda3}\left(\frac{\partial\Pi^\beta_\lambda}{\partial z} + \frac{1}{h_\lambda}\frac{\partial\Pi^\beta_3}{\partial y_\lambda}\right) = 0 \qquad z = z^\pm\end{aligned} \tag{29}$$

3.3.2. In-plane (stretch and shear) local problem U(y,z)

Assume a pure in-plane case that $\gamma = \kappa = 0$. (9) and (15) lead to

$$\begin{aligned}
&\frac{1}{h_\mu}\frac{\partial}{\partial y_\mu}\left[c_{\mu 3 v 3}\left(\frac{\partial U_\mu^{\alpha\beta}}{\partial z}+\frac{1}{h_v}\frac{\partial U_3^{\alpha\beta}}{\partial y_v}\right)\right]+\frac{\partial}{\partial z}\left(c_{33\alpha\beta}+c_{33v\lambda}\frac{1}{h_\lambda}\frac{\partial U_v^{\alpha\beta}}{\partial y_\lambda}+c_{3333}\frac{\partial U_3^{\alpha\beta}}{\partial z}\right)=0\\
&\frac{1}{h_\mu}\frac{\partial}{\partial y_\mu}\left(c_{v\mu\alpha\beta}+c_{v\mu 33}\frac{\partial U_3^{\alpha\beta}}{\partial z}+c_{v\mu v\lambda}\frac{1}{h_\lambda}\frac{\partial U_v^{\alpha\beta}}{\partial y_\lambda}\right)+\frac{\partial}{\partial z}\left[c_{v3\omega 3}\left(\frac{\partial U_\omega^{\alpha\beta}}{\partial z}+\frac{1}{h_\omega}\frac{\partial U_3^{\alpha\beta}}{\partial y_\omega}\right)\right]=0
\end{aligned} \tag{30}$$

The boundary conditions are

$$\begin{aligned}
&c_{33\alpha\beta}+c_{33v\lambda}\frac{1}{h_\lambda}\frac{\partial U_v^{\alpha\beta}}{\partial y_\lambda}+c_{3333}\frac{\partial U_3^{\alpha\beta}}{\partial z}=0 \qquad z=z^{\pm}\\
&c_{v3\omega 3}\left(\frac{\partial U_\omega^{\alpha\beta}}{\partial z}+\frac{1}{h_\omega}\frac{\partial U_3^{\alpha\beta}}{\partial y_\omega}\right)=0 \qquad z=z^{\pm}
\end{aligned} \tag{31}$$

3.3.3. Flexural local problem V(y,z)

Similarly, the equilibrium equations and boundary conditions are given as

$$\begin{aligned}
&\frac{1}{h_\mu}\frac{\partial}{\partial y_\mu}\left[c_{\mu 3 v 3}\left(\frac{\partial V_\mu^{\alpha\beta}}{\partial z}+\frac{1}{h_v}\frac{\partial V_3^{\alpha\beta}}{\partial y_v}\right)\right]+\frac{\partial}{\partial z}\left(zc_{33\alpha\beta}+c_{33v\lambda}\frac{1}{h_\lambda}\frac{\partial V_v^{\alpha\beta}}{\partial y_\lambda}+c_{3333}\frac{\partial V_3^{\alpha\beta}}{\partial z}\right)=0\\
&\frac{1}{h_\mu}\frac{\partial}{\partial y_\mu}\left(zc_{v\mu\alpha\beta}+c_{v\mu 33}\frac{\partial V_3^{\alpha\beta}}{\partial z}+c_{v\mu v\lambda}\frac{1}{h_\lambda}\frac{\partial V_v^{\alpha\beta}}{\partial y_\lambda}\right)+\frac{\partial}{\partial z}\left[c_{v3\omega 3}\left(\frac{\partial V_\omega^{\alpha\beta}}{\partial z}+\frac{1}{h_\omega}\frac{\partial V_3^{\alpha\beta}}{\partial y_\omega}\right)\right]=0
\end{aligned} \tag{32}$$

$$\begin{aligned}
&zc_{33\alpha\beta}+c_{33v\lambda}\frac{1}{h_\lambda}\frac{\partial V_v^{\alpha\beta}}{\partial y_\lambda}+c_{3333}\frac{\partial V_3^{\alpha\beta}}{\partial z}=0 \qquad z=z^{\pm}\\
&c_{v3\omega 3}\left(\frac{\partial V_\omega^{\alpha\beta}}{\partial z}+\frac{1}{h_\omega}\frac{\partial V_3^{\alpha\beta}}{\partial y_\omega}\right)=0 \qquad z=z^{\pm}
\end{aligned} \tag{33}$$

4. Analytical approach—multi-pass homogenization technique

In engineering applications of homogenization theory, the exact analytical solutions are seldom obtainable and the approximations are usually made either by semi-analytical method or by pure numerical techniques such as finite element method. In the problem of honeycomb cells, there are 3-D local functions (see Eqs. (28)–(33)) physically interpreted as complicated combination of local warping, stretching, bending, shearing, and twisting, etc. The exact mathematical expression for each of the functions is almost impossible to derive analytically. As demonstrated in (24), fortunately, weak solutions are sufficient when the homogenized properties are sought in a variational sense.

For even a weak solution of the local problem as (28)–(33), their 3-D deformations are difficult to deal with, and the direct construction of cell plates' displacement (Hohe and Becker, 2001) involves relatively complicated and implicit numerical process. Hereby in the first pass of the MPH, a simplified GTM is proposed that a spatial heterogeneous problem can be transferred into a material heterogeneous problem with consequent intermediate equivalent properties. By this way, the strain energy of cell walls can be completely expressed by the resulting intermediate equivalent stiffness without omitting small higher order

terms, as exemplified by Φ_1 and Φ_2 in Eqs. (65) and (70) of Section 4.2.2. Note in the GTM there is no restriction about the thickness of cell walls, as long as energy equivalence is satisfied with appropriate derivations of intermediate equivalent stiffness. In the second pass, the 2-D heterogeneous problem then can be analytically homogenized in a unit cell by the variational approximations of displacement field with Rayleigh–Ritz method or partition method, etc. The weak form solution of the partial differential equations is finally verified with the FEA results in Section 5.

The MPH technique originates from the idea that the homogenization of an object may be processed by its principal axes one by one, i.e., the homogenized results obtained along one axis can be well applied to the second pass along another axis. There are several engineering applications of the MPH technique, (e.g., Astley et al., 1997). The separation of the process is found very effective in the homogenization of honeycomb cells, as evidenced in this paper. To illustrate the whole process explicitly, a better way is to follow an analytical example as given in Section 4, rather than general procedure description. Hereby the most used hexagonal honeycomb is taken as an example (Figs. 4 and 5), which has been given the most attention in honeycomb studies with much available theoretical and experimental data.

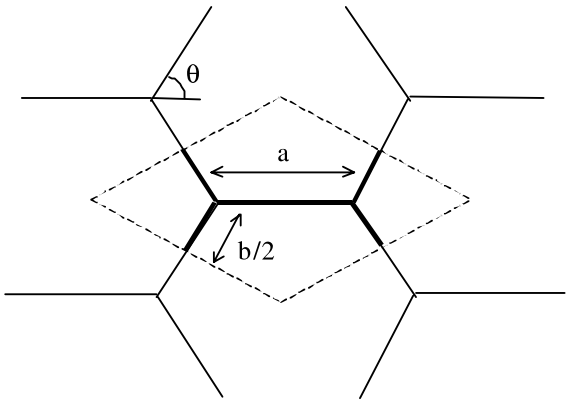

Fig. 4. Hexagonal core configuration.

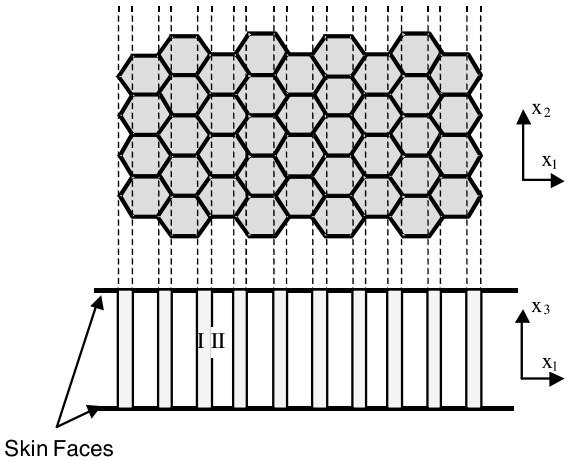

Fig. 5. GTM—first pass of MPH technique.

4.1. First pass—geometry-to-material transformation model

In principle by the GTM, a doubly periodic sandwich panel is transformed into a 1-D periodic panel. For hexagons shown in Fig. 5, the plate thus becomes consisting of two alternative thin sandwich beams with their intermediate equivalent material properties. In the first pass the GTM homogenization is made along, say x_2, so that the information of spatial periodicity along x_2 is stored in the consequent intermediate equivalent stiffness. The resulting 2-D heterogeneous composite then can be conveniently assessed in the second pass along x_1.

For simplicity, the cell walls and skin faces are assumed both made of isotropic materials, where Young's modulus, shear modulus and Poisson's ratio are denoted E_c, G_c, v_c and E_f, G_f, v_f, respectively. Geometrical notations of the hexagon are illustrated in Fig. 4. It should be pointed out that for anisotropic materials the procedure is kept identical. The example is confined to transversely symmetric sandwiches with thin-walled hexagonal core to which the thin beam model (Gibson and Ashby, 1988) can be applied.

With the above assumptions, the faces of the two thin sandwich beams are known homogeneous so that structural homogenization only needs to be processed on two types of beam cores, I and II (Fig. 5). The intermediate equivalent properties may be obtained following the principle of structural mechanics, and the derivation refers to similar problems detailed in Gibson and Ashby (1988) and Masters and Evans (1996). The properties of core II consisting of parallel cell walls are

$$\begin{aligned}
&E_1^{hc2} = \frac{1}{2\sin\theta}\frac{t_2}{b}E_c, \qquad E_2^{hc2} \approx 0, \qquad E_3^{hc2} = \frac{1}{2\sin\theta}\frac{t_2}{b}E_c \\
&G_{13}^{hc2} = \frac{1}{2\sin\theta}\frac{t_2}{b}G_c, \qquad G_{23}^{hc2} \approx 0, \qquad G_{12}^{hc2} = \frac{a/b+\cos\theta}{(a/b)^2(1+2a/b)\sin\theta}\left(\frac{t_2}{b}\right)^3 E_c \\
&v_{12}^{hc2} \approx v_{21}^{hc2} \approx 0, \qquad v_{31}^{hc2} = v_{13}^{hc2} = v_c, \qquad v_{23}^{hc2} \approx v_{23}^{hc2} \approx 0
\end{aligned} \tag{34}$$

And the properties of core I with folded cell walls are

$$\begin{aligned}
&E_1^{hc1} = \frac{\cos\theta}{\sin^3\theta[1+ctg^2\theta(t_1/b)^2]}\left(\frac{t_1}{b}\right)^3 E_c \\
&E_2^{hc1} = \frac{\sin\theta}{\cos^3\theta[1+tg^2\theta(t_1/b)^2]}\left(\frac{t_1}{b}\right)^3 E_c, \qquad E_3^{hc1} = \frac{1}{\sin\theta\cos\theta}\frac{t_1}{b}E_c \\
&G_{13}^{hc1} = ctg\theta\frac{t_1}{b}G_c, \qquad G_{23}^{hc1} = tg\theta\frac{t_1}{b}G_c, \qquad G_{12}^{hc1} = \sin\theta\cos\theta\frac{t_1}{b}E_c \\
&v_{12}^{hc1} = ctg^2\theta\frac{1-(t_1/b)^2}{1+ctg^2\theta(t_1/b)^2}, \qquad v_{21}^{hc1} = tg^2\theta\frac{1-(t_1/b)^2}{1+tg^2\theta(t_1/b)^2} \\
&v_{31}^{hc1} = v_c\cos\theta, \qquad v_{13}^{hc1} = \frac{\cos^3\theta}{\sin^2\theta[1+ctg^2\theta(t_1/b)^2]}\left(\frac{t_1}{b}\right)^2 v_c \\
&v_{32}^{hc1} = v_c\sin\theta, \qquad v_{23}^{hc1} = \frac{\sin^3\theta}{\cos^2\theta[1+tg^2\theta(t_1/b)^2]}\left(\frac{t_1}{b}\right)^2 v_c
\end{aligned} \tag{35}$$

where the superscript h denotes intermediate core equivalent properties, and c, 1, 2 for core and its type I, II, respectively.

Note that calculation of in-plane Poisson's ratios, with such equations as (4.13–14) in Gibson and Ashby (1988), would result in-plane stiffness much deviated from true values, and even produce singularities. The correct way is to further consider the stretch deformation, as noticed by Warren and Kraynik (1987) and Masters and Evans (1996). The formulas of Poisson's ratios in (35) are derivable from (4.50) in Gibson and Ashby (1988).

The generalized Hooke's law for the above hexagons with three planes of the elastic symmetry can be written in terms of the intermediate properties of principal elastic constants (Lekhnitskii, 1968)

$$\begin{aligned}
\varepsilon_1^h &= \frac{1}{E_1^h}\sigma_1^h - \frac{\nu_{21}^h}{E_2^h}\sigma_2^h - \frac{\nu_{31}^h}{E_3^h}\sigma_3^h, \qquad \gamma_{23}^h = \frac{1}{G_{23}^h}\tau_{23}^h \\
\varepsilon_2^h &= -\frac{\nu_{12}^h}{E_1^h}\sigma_1^h + \frac{1}{E_2^h}\sigma_2^h - \frac{\nu_{32}^h}{E_3^h}\sigma_3^h, \qquad \gamma_{13}^h = \frac{1}{G_{13}^h}\tau_{13}^h \\
\varepsilon_3^h &= -\frac{\nu_{13}^h}{E_1^h}\sigma_1^h - \frac{\nu_{23}^h}{E_2^h}\sigma_2^h + \frac{1}{E_3^h}\sigma_3^h, \qquad \gamma_{12}^h = \frac{1}{G_{12}^h}\tau_{12}^h
\end{aligned} \tag{36}$$

And the inverse of (36) results in the expression of stress variables

$$\begin{aligned}
\sigma_1^h &= \frac{E_1^h}{1-\Delta}\left[(1-\nu_{23}^h\nu_{32}^h)\varepsilon_1^h + (\nu_{21}^h+\nu_{23}^h\nu_{31}^h)\varepsilon_2^h + (\nu_{31}^h+\nu_{21}^h\nu_{32}^h)\varepsilon_3^h\right], \qquad \tau_{23}^h = G_{23}^h\gamma_{23}^h \\
\sigma_2^h &= \frac{E_2^h}{1-\Delta}\left[(1-\nu_{13}^h\nu_{31}^h)\varepsilon_2^h + (\nu_{12}^h+\nu_{13}^h\nu_{32}^h)\varepsilon_1^h + (\nu_{32}^h+\nu_{12}^h\nu_{31}^h)\varepsilon_3^h\right], \qquad \tau_{13}^h = G_{13}^h\gamma_{13}^h \\
\sigma_3^h &= \frac{E_3^h}{1-\Delta}\left[(1-\nu_{12}^h\nu_{21}^h)\varepsilon_3^h + (\nu_{23}^h+\nu_{21}^h\nu_{13}^h)\varepsilon_2^h + (\nu_{13}^h+\nu_{12}^h\nu_{23}^h)\varepsilon_1^h\right], \qquad \tau_{12}^h = G_{12}^h\gamma_{12}^h \\
\Delta &= \nu_{12}^h\nu_{21}^h + \nu_{13}^h\nu_{31}^h + \nu_{23}^h\nu_{32}^h + \nu_{12}^h\nu_{23}^h\nu_{31}^h + \nu_{13}^h\nu_{21}^h\nu_{32}^h
\end{aligned} \tag{37}$$

4.2. Second pass—2-D unit cell homogenization

After the cores I and II are homogenized in x_2 as done in the first pass, a 3-D local problem is thus simplified into a 2-D problem as shown in Fig. 6. There are three regions, i.e., core I, core II, and two skin faces III, forming a three-phase homogenization problem with governing equations (28)–(33). The material properties of the regions I and II are orthotropic and the region III isotropic, which henceforth are expressed by engineering constants, Young's modulus E, shear modulus G, and Poisson's ratio ν. Note for sandwich panels the following analyses in plane y_1–z are of plane-strain deformations.

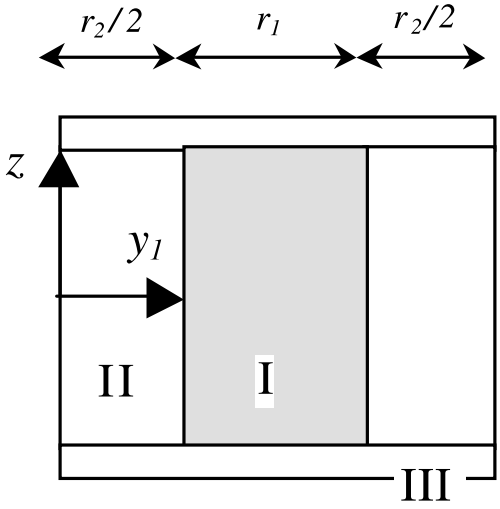

Fig. 6. Second pass of MPH technique.

4.2.1. Homogenized transverse shear stiffness

Denote the core thickness as c, the period of honeycomb as $l_0 = a + b\cos\theta$ (Fig. 4), and define the ratio $r_1 = b\cos\theta/l_0$, $r_2 = a/l_0$, $0 < r_1, r_2 < 1$, $r_1 + r_2 = 1$. Here h_1 for hexagons equals l_0/c. From (28) and (37) with $\varepsilon_2^h = 0$, the field equations for the regions I and II may be given as

$$\begin{aligned}
&G_{13}^{hc\alpha}\left(\frac{\partial^2\Pi_1^{[\alpha]}}{\partial z^2}+\frac{1}{h_1}\frac{\partial^2\Pi_3^{[\alpha]}}{\partial y_1\partial z}\right)+\frac{E_1^{hc\alpha}}{1-\Delta^{[\alpha]}}\left[(v_{31}^{hc\alpha}+v_{21}^{hc\alpha}v_{32}^{hc\alpha})\frac{1}{h_1}\frac{\partial^2\Pi_3^{[\alpha]}}{\partial y_1\partial z}+(1-v_{32}^{hc\alpha}v_{23}^{hc\alpha})\frac{1}{h_1^2}\frac{\partial^2\Pi_1^{[\alpha]}}{\partial y_1^2}\right]=0\\
&G_{13}^{hc\alpha}\left(\frac{1}{h_1}\frac{\partial^2\Pi_1^{[\alpha]}}{\partial y_1\partial z}+\frac{1}{h_1^2}\frac{\partial^2\Pi_3^{[\alpha]}}{\partial y_1^2}\right)+\frac{E_3^{hc\alpha}}{1-\Delta^{[\alpha]}}\left[(v_{13}^{hc\alpha}+v_{12}^{hc\alpha}v_{23}^{hc\alpha})\frac{1}{h_1}\frac{\partial^2\Pi_1^{[\alpha]}}{\partial y_1\partial z}+(1-v_{12}^{hc\alpha}v_{21}^{hc\alpha})\frac{\partial^2\Pi_3^{[\alpha]}}{\partial z^2}\right]=0\\
&\Delta^{[\alpha]}=v_{12}^{hc\alpha}v_{21}^{hc\alpha}+v_{13}^{hc\alpha}v_{31}^{hc\alpha}+v_{23}^{hc\alpha}v_{32}^{hc\alpha}+v_{12}^{hc\alpha}v_{23}^{hc\alpha}v_{31}^{hc\alpha}+v_{13}^{hc\alpha}v_{21}^{hc\alpha}v_{32}^{hc\alpha}
\end{aligned}\tag{38}$$

where $\alpha = 1$ or 2 denotes the region I or II, respectively.

The left and right boundary conditions for the regions I and II are the continuity and the periodicity conditions for both stress and displacement fields. The top and bottom boundary conditions are the interactions between core and skin faces, which are complicatedly involved with faces internal fields. To simplify them, the approximation is made that faces are assumed infinite rigid, as those of Kelsey et al. (1958) and Penzien and Didriksson (1964), by which $\Pi_3^{[\alpha]}$ becomes zero at top and bottom interfaces. Among all admissible displacement fields satisfying above conditions, the following one in Fourier series is given, based on the symmetric material and the anti-symmetric loading about the panel middle plane

$$\begin{aligned}
&\Pi_1^{[1]}=0\\
&\Pi_3^{[1]}=\sum_n a_n^{[1]}\sinh\left[\lambda_n^{[1]}h_1\left(y_1-\frac{1}{2}\right)\right]\cos(n\pi z),\quad n=1,3,5\ldots\\
&\Pi_1^{[2]}=0\\
&\Pi_3^{[2]}=\sum_n a_n^{[2]}\sinh(\lambda_n^{[2]}h_1y_1)\cos(n\pi z),\quad n=1,3,5\ldots
\end{aligned}\tag{39}$$

Substituting (39) into the second equation of (38) results in eigenvalues

$$\begin{aligned}
\lambda_n^{[1]}&=n\pi\sqrt{\frac{E_3^{hc1}(1-v_{12}^{hc1}v_{21}^{hc1})}{G_{13}^{hc1}(1-\Delta^{[1]})}}\\
\lambda_n^{[2]}&=n\pi\sqrt{\frac{E_3^{hc2}(1-v_{12}^{hc2}v_{21}^{hc2})}{G_{13}^{hc2}(1-\Delta^{[2]})}}
\end{aligned}\tag{40}$$

And the first equation of (38) is satisfied by variational partition method in a weak form since

$$\begin{aligned}
&\sum_n\int_{y_1}\int_{-1/2}^{1/2}\cosh\left[\lambda_n^{[1]}h_1\left(y_1-\frac{l_0}{2}\right)\right]\sin(n\pi z)\,\mathrm{d}y_1\,\mathrm{d}z=0,\quad n=1,3,5\ldots\\
&\sum_n\int_{y_1}\int_{-1/2}^{1/2}\cosh(\lambda_n^{[2]}h_1y_1)\sin(n\pi z)\,\mathrm{d}y_1\,\mathrm{d}z=0,\quad n=1,3,5\ldots
\end{aligned}\tag{41}$$

To find the coefficients a_n, we impose displacement continuity conditions between the region I and II

$$\Pi_3^{[1]}=\Pi_3^{[2]}\quad\text{at } y_1=r_2/2\tag{42}$$

and the equilibrium condition of shear stress

$$G_{13}^{hc1}\left(1+\frac{1}{h_1}\frac{\partial \Pi_3^{[1]}}{\partial y_1}\right)=G_{13}^{hc2}\left(1+\frac{1}{h_1}\frac{\partial \Pi_3^{[2]}}{\partial y_1}\right)\quad \text{at } y_1=r_2/2 \tag{43}$$

Note the continuity condition of normal stress is satisfied variationally by (41). With the conditions (42) and (43), the coefficients are obtained

$$\begin{aligned} a_n^{[1]} &= \frac{4\left(G_{13}^{hc1}-G_{13}^{hc2}\right)\sinh\left(\lambda_n^{[1]}h_1\frac{r_1}{2}\right)}{n\pi\left[-G_{13}^{hc2}\lambda_n^{[2]}\cosh\left(\lambda_n^{[2]}h_1\frac{r_1}{2}\right)\sinh\left(\lambda_n^{[1]}\frac{h_1r_2}{2}\right)+G_{13}^{hc1}\lambda_n^{[1]}\cosh\left(\lambda_n^{[1]}\frac{h_1r_2}{2}\right)\sinh\left(\lambda_n^{[2]}h_1\frac{r_1}{2}\right)\right]} \\ a_n^{[2]} &= \frac{4\left(G_{13}^{hc2}-G_{13}^{hc1}\right)\sinh\left(\lambda_n^{[1]}\frac{h_1r_2}{2}\right)}{n\pi\left[-G_{13}^{hc2}\lambda_n^{[2]}\cosh\left(\lambda_n^{[2]}h_1\frac{r_1}{2}\right)\sinh\left(\lambda_n^{[1]}\frac{h_1r_2}{2}\right)+G_{13}^{hc1}\lambda_n^{[1]}\cosh\left(\lambda_n^{[1]}\frac{h_1r_2}{2}\right)\sinh\left(\lambda_n^{[2]}h_1\frac{r_1}{2}\right)\right]} \end{aligned} \tag{44}$$

From (23), (26), (27) and (37), the homogenized transverse shear stiffness is expressed

$$H_{55}^H=c\langle C_{1313}\rangle=cG_{13}^H$$

where

$$G_{13}^H=2\int_0^{r_2/2}\int_{-1/2}^{1/2}G_{13}^{hc2}\left(1+\frac{1}{h_1}\frac{\partial \Pi_3^{[2]}}{\partial y_1}\right)\mathrm{d}z\,\mathrm{d}y_1+2\int_{r_2/2}^{1/2}\int_{-1/2}^{1/2}G_{13}^{hc1}\left(1+\frac{1}{h_1}\frac{\partial \Pi_3^{[1]}}{\partial y_1}\right)\mathrm{d}z\,\mathrm{d}y_1 \tag{45}$$

And the integration of (45) results

$$G_{13}^H=\sum_{n=1,3,5\ldots}\frac{4(-1)^{\frac{n-1}{2}}}{n^2\pi^2}\left[G_{13}^{hc1}r_1+G_{13}^{hc2}r_2+a_n^{[2]}G_{13}^{hc1}\frac{n\pi}{h_1}\sinh\left(\frac{r_1}{2}h_1\lambda_n^{[1]}\right)+a_n^{[1]}G_{13}^{hc2}\frac{n\pi}{h_1}\sinh\left(\frac{r_2}{2}h_1\lambda_n^{[2]}\right)\right] \tag{46}$$

The above formula (46) can be easily calculated with a symbolic mathematical program, such as *Mathematica* or *Maple*. Hereby the numerical results are given in Table 1 for two configurations of hexagons as function of core thickness ratio h_1.

For regular hexagons with $t_2=2t_1$, $a=b$, $\theta=60^\circ$, the ratio of $r_2=2/3$, and the isotropic material with Poisson's ratio of 0.3, the intermediate equivalent properties of the regions I and II are obtained from (34) and (35)

Table 1
Normalized homogenized transverse shear stiffness G_{13}^H/G_{13}^{hc1}

h_1	LB	1/100	1/20	1/10	1/8	1/6	1/5	1/4	1/3	1/2	1	2	10	UB
$r_2=2/3$	1.500	1.500	1.504	1.508	1.510	1.514	1.517	1.521	1.529	1.543 (1.544)	1.580 (1.584)	1.618	1.656	1.666
$r_2=0.536$	1.366	1.366	1.370	1.374	1.377	1.381	1.384	1.388	1.395	1.410	1.448	1.486	1.525	1.536

Note: the numbers based on FEA are given in parentheses.

$$
\begin{aligned}
&E_3^{hc1} = 5.2G_{13}^{hc1}, \qquad G_{13}^{hc1} = \frac{t_1}{\sqrt{3}b}G^c \\
&E_3^{hc2} = 5.2G_{13}^{hc1}, \qquad G_{13}^{hc2} = 2G_{13}^{hc1} \\
&\frac{1-v_{12}^{hc2}v_{21}^{hc2}}{1-\Delta^{[2]}} = 1.0989 \\
&\frac{1-v_{12}^{hc1}v_{21}^{hc1}}{1-\Delta^{[1]}} = 1.0571 \quad \text{for } \frac{t_1}{b} \leqslant 0.1
\end{aligned}
\tag{47}
$$

Further consider a group of irregular hexagons with $t_2 = 2t_1$, $a = b$, $\theta = 30^\circ$ and the ratio of $r_2 = 0.536$. The properties of the regions I and II are the same as (47), wherein noticed that the value of $1 - v_{12}^{hc1}v_{21}^{hc1}/1 - \Delta^{[1]}$ does not change. The results of two groups are shown in Table 1 and graphically in Figs. 7 and 8.

Remarks

(a) The variational principle leads to the LB and UB of shear stiffness as derived first by Kelsey et al. (1958), and later by Gibson and Ashby (1988) and Shi and Tong (1995a). With the simple application of

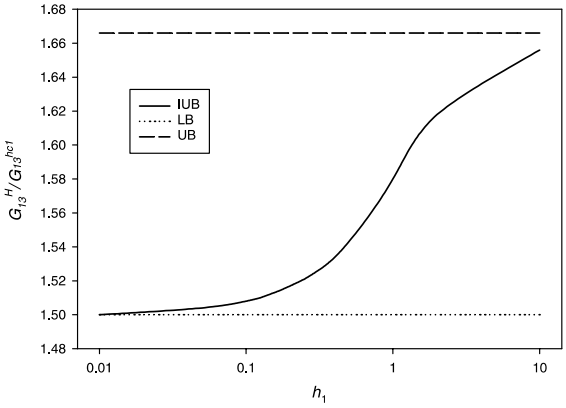

Fig. 7. Transverse shear stiffness G_{13}^H with $r_2 = 2/3$.

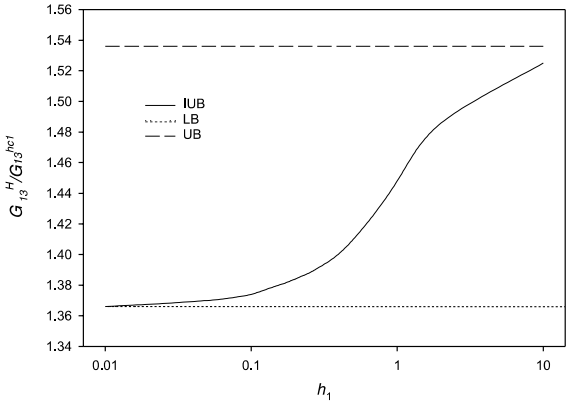

Fig. 8. Transverse shear stiffness G_{13}^H with $r_2 = 0.536$.

Reuss Model and Voigt Model for the 2-D unit cell in Fig. 6, respectively, the formulas for UB and LB can be written as

$$G_{13}^{H}\big|_{\mathrm{UB}} = r_1 G_{13}^{hc1} + r_2 G_{13}^{hc2}$$
$$G_{13}^{H}\big|_{\mathrm{LB}} = \frac{G_{13}^{hc1} G_{13}^{hc2}}{r_1 G_{13}^{hc2} + r_2 G_{13}^{hc1}} \tag{48}$$

Note the two bounds are not functions of h_1. The substitution of (34), (35) into (48) leads to the formulas of LB and UB as function of geometrical parameters

$$G_{13}^{H}\big|_{\mathrm{UB}} = \frac{2t_1 b\cos^2\theta + t_2 a}{2b\sin\theta(a + b\cos\theta)} G_c$$
$$G_{13}^{H}\big|_{\mathrm{LB}} = \frac{b\cos\theta + a}{b\sin\theta(b/t_1 + 2a/t_2)} G_c \tag{49}$$

which are identical to those formulas given in the literature (Kelsey, 1958; Gibson and Ashby, 1988; etc.).

(b) Penzien and Didriksson (1964) gave a similar result as (46); however its assumption of infinite Young's modulus in y_1-axis is not right, which is corrected in this study by the GTM and the weak form solution. Further we should point out that the semi-analytical approximation in Section 4.2.1 gives an improved upper bound (IUB) since skin faces are assumed infinite rigid. As shown in Figs. 7 and 8, the IUB value converges to the two bounds when $h_1 \to 0$ or ∞, which confirms the solution.

The FEA results in Section 5 have two cases ($h_1 = 1$ and 1/2) illogically a little higher than IUB values, as modified in Table 1. The reason is attributed to the inconsistency between the IUB displacement field (39) and FEA modeling on the rigid assumption of skin–core joints. This influence, however, is quite small, and therefore, IUB approximation of (46) is recommended as an effective formula that can be further combined with Eq. (91) for design and optimization. For common hexagons with $h_1 < 1$, the LB value can be conservatively used in preliminary design. For refined sandwich analysis, such as FEA modeling, more accurate shear stiffness is necessary; thus (46) and (91) or unit cell FEA approach can be useful.

(c) When skin effect is not taken into account (i.e., there is no normal constraint at the top and bottom boundaries), with continuity conditions (42) and (43) the exact solution of (38) may be simply expressed as

$$\Pi_1^{[1]} = 0$$
$$\Pi_3^{[1]} = \frac{h_1(G_{13}^{hc2} - G_{13}^{hc1})}{\frac{r_2}{r_1} G_{13}^{hc2} + G_{13}^{hc1}} y_1 + \text{constant}$$
$$\Pi_1^{[2]} = 0$$
$$\Pi_3^{[2]} = \frac{h_1(G_{13}^{hc1} - G_{13}^{hc2})}{G_{13}^{hc2} + \frac{r_1}{r_2} G_{13}^{hc1}} y_1 \tag{50}$$

It can be easily checked that the substitution of (50) into (45) results in the identical expression as (49), which in turn validates the IUB approach.

(d) From the GTM in Section 4.1, the other homogenized transverse shear stiffness G_{23}^{H} can be derived with parallel model or Reuss model

$$G_{23}^{H} = r_1 G_{23}^{hc1} + r_2 G_{23}^{hc2} \tag{51}$$

and the substitution of (34) and (35) into (51) gives

$$G_{23}^{H} = \frac{b\sin\theta}{b\cos\theta + a} \frac{t_1}{b} G_c \tag{52}$$

Clearly there is no skin effect for the case of G_{23}^{H}, which can also be intuitively seen from the GTM in Fig. 5.

(e) For common honeycomb sandwiches, the thickness of skin faces is small in relation to that of core, whilst the shear modulus of the former is much higher. Owning to this fact, the equivalent shear stiffness of the sandwiches is overwhelmingly determined by core properties. To further take the thickness of skin faces t_f into account, the unit width transverse shear stiffness of a sandwich panel can be written as per Allen (1969)

$$\begin{aligned} H_{55} &= \frac{(t_f + c)^2}{c} G_{13}^H \\ H_{44} &= \frac{(t_f + c)^2}{c} G_{23}^H \end{aligned} \tag{53}$$

4.2.2. Homogenized in-plane stretch stiffness

The governing field equations and the boundary conditions are the same as (38) and those of Section 4.2.1

$$\begin{aligned} &G_{13}^{hc\alpha}\left(\frac{\partial^2 U_1^{[\alpha]}}{\partial z^2} + \frac{1}{h_1}\frac{\partial^2 U_3^{[\alpha]}}{\partial y_1 \partial z}\right) + \frac{E_1^{hc\alpha}}{1 - \Delta^{[\alpha]}}\left[(\nu_{31}^{hc\alpha} + \nu_{21}^{hc\alpha}\nu_{32}^{hc\alpha})\frac{1}{h_1}\frac{\partial^2 U_3^{[\alpha]}}{\partial y_1 \partial z} + (1 - \nu_{32}^{hc\alpha}\nu_{23}^{hc\alpha})\frac{1}{h_1^2}\frac{\partial^2 U_1^{[\alpha]}}{\partial y_1^2}\right] = 0 \\ &G_{13}^{hc\alpha}\left(\frac{1}{h_1}\frac{\partial^2 U_1^{[\alpha]}}{\partial y_1 \partial z} + \frac{1}{h_1^2}\frac{\partial^2 U_3^{[\alpha]}}{\partial y_1^2}\right) + \frac{E_3^{hc\alpha}}{1 - \Delta^{[\alpha]}}\left[(\nu_{13}^{hc\alpha} + \nu_{12}^{hc\alpha}\nu_{23}^{hc\alpha})\frac{1}{h_1}\frac{\partial^2 U_1^{[\alpha]}}{\partial y_1 \partial z} + (1 - \nu_{12}^{hc\alpha}\nu_{21}^{hc\alpha})\frac{\partial^2 U_3^{[\alpha]}}{\partial z^2}\right] = 0 \\ &\Delta^{[\alpha]} = \nu_{12}^{hc\alpha}\nu_{21}^{hc\alpha} + \nu_{13}^{hc\alpha}\nu_{31}^{hc\alpha} + \nu_{23}^{hc\alpha}\nu_{32}^{hc\alpha} + \nu_{12}^{hc\alpha}\nu_{23}^{hc\alpha}\nu_{31}^{hc\alpha} + \nu_{13}^{hc\alpha}\nu_{21}^{hc\alpha}\nu_{32}^{hc\alpha} \end{aligned} \tag{54}$$

Due to the loading condition, the solution approximation is made in reverse to the case in Section 4.2.1, i.e., in this case the displacement is ensured to satisfy governing equations strictly in y_1 and weakly in z. By the doubly symmetry of material and loading, the displacement field is constructed as

$$\begin{aligned} U_1^{[1]} &= \sum_n b_n^{[1]} \sinh\left[\lambda_n^{[1]} h_1\left(y_1 - \frac{1}{2}\right)\right]\cos(n\pi z), \quad n = 1, 3, 5\ldots \\ U_3^{[1]} &= \sum_n c_n \sin(n\pi z), \quad n = 1, 3, 5\ldots \\ U_1^{[2]} &= \sum_n b_n^{[2]} \sinh\left(\lambda_n^{[2]} h_1 y_1\right)\cos(n\pi z), \quad n = 1, 3, 5\ldots \\ U_3^{[2]} &= \sum_n c_n \sin(n\pi z), \quad n = 1, 3, 5\ldots \end{aligned} \tag{55}$$

The substitution of (55) into the first equation of (54) leads to eigenvalues

$$\begin{aligned} \lambda_n^{[1]} &= n\pi\sqrt{\frac{G_{13}^{hc1}(1 - \Delta^{[1]})}{E_1^{hc1}(1 - \nu_{23}^{hc1}\nu_{32}^{hc1})}} \\ \lambda_n^{[2]} &= n\pi\sqrt{\frac{G_{13}^{hc2}(1 - \Delta^{[2]})}{E_1^{hc2}(1 - \nu_{23}^{hc2}\nu_{32}^{hc2})}} \end{aligned} \tag{56}$$

Note in (55) that there are three unknown coefficients, and the second equation of (54) cannot be simply satisfied by partition method in weak form as (41). An effective approach is to follow the Rayleigh–Ritz Method that is convenient to treat orthonormal series. The quadratic energy functional of (54) is given by

$$I(U) = Q_s + Q_y + Q_z$$

$$Q_s = 2\int_{-1/2}^{1/2}\int_{0}^{r_2/2} \frac{1}{2} G_{13}^{hc2}\left(\frac{\partial U_1^{[2]}}{\partial z} + \frac{1}{h_1}\frac{\partial U_3^{[2]}}{\partial y_1}\right)^2 \mathrm{d}y_1\,\mathrm{d}z + 2\int_{-1/2}^{1/2}\int_{r_2/2}^{1/2} \frac{1}{2} G_{13}^{hc1}\left(\frac{\partial U_1^{[1]}}{\partial z} + \frac{1}{h_1}\frac{\partial U_3^{[1]}}{\partial y_1}\right)^2 \mathrm{d}y_1\,\mathrm{d}z$$

$$Q_y = 2\int_{-1/2}^{1/2}\int_{0}^{r_2/2} \frac{1}{2}\frac{E_1^{hc2}}{1-\Delta^{[2]}}\left[(v_{31}^{hc2} + v_{21}^{hc2}v_{32}^{hc2})\frac{\partial U_3^{[2]}}{\partial z} + (1 - v_{23}^{hc2}v_{32}^{hc2})\left(\frac{1}{h_1}\frac{\partial U_1^{[2]}}{\partial y_1} + 1\right)\right]\left(\frac{1}{h_1}\frac{\partial U_1^{[2]}}{\partial y_1} + 1\right)\mathrm{d}y_1\,\mathrm{d}z$$

$$+ 2\int_{-1/2}^{1/2}\int_{r_2/2}^{1/2} \frac{1}{2}\frac{E_1^{hc1}}{1-\Delta^{[1]}}\left[(v_{31}^{hc1} + v_{21}^{hc1}v_{32}^{hc1})\frac{\partial U_3^{[1]}}{\partial z} + (1 - v_{23}^{hc1}v_{32}^{hc1})\frac{1}{h_1}\frac{\partial U_1^{[1]}}{\partial y_1} + 1\right]\left(\frac{1}{h_1}\frac{\partial U_1^{[1]}}{\partial y_1} + 1\right)\mathrm{d}y_1\,\mathrm{d}z$$

$$Q_z = 2\int_{-1/2}^{1/2}\int_{0}^{r_2/2} \frac{1}{2}\frac{E_3^{hc2}}{1-\Delta^{[2]}}\left[(v_{13}^{hc2} + v_{12}^{hc2}v_{23}^{hc2})\left(\frac{1}{h_1}\frac{\partial U_1^{[2]}}{\partial y_1} + 1\right) + (1 - v_{21}^{hc2}v_{12}^{hc2})\frac{\partial U_3^{[2]}}{\partial z}\right]\frac{\partial U_3^{[2]}}{\partial z}\,\mathrm{d}y_1\,\mathrm{d}z$$

$$+ 2\int_{-1/2}^{1/2}\int_{r_2/2}^{1/2} \frac{1}{2}\frac{E_3^{hc1}}{1-\Delta^{[1]}}\left[(v_{13}^{hc1} + v_{12}^{hc1}v_{23}^{hc1})\left(\frac{1}{h_1}\frac{\partial U_1^{[1]}}{\partial y_1} + 1\right) + (1 - v_{21}^{hc1}v_{12}^{hc1})\frac{\partial U_3^{[1]}}{\partial z}\right]\frac{\partial U_3^{[1]}}{\partial z}\,\mathrm{d}y_1\,\mathrm{d}z \tag{57}$$

where Q_s, Q_y, and Q_z denote strain energy in shear, y_1-normal, and z-normal, respectively.

The three equations for three unknown coefficients are the displacement continuity condition between regions I and II

$$U_1^{[1]} = U_1^{[2]} \quad \text{at } y_1 = r_2/2 \tag{58}$$

and the differentiation of functional $I(U)$ about any two unknowns, say two b_n

$$\begin{aligned} \frac{\partial I(U)}{\partial b_n^{[1]}} &= 0 \\ \frac{\partial I(U)}{\partial b_n^{[2]}} &= 0 \end{aligned} \tag{59}$$

The substitution of (55) and (57) into (58) and (59) solves the three coefficients, where the symbolic calculation can be conveniently carried out by *Mathematica* or *Maple*. The results for the coefficients b_n and c_n are omitted here due to their lengthy symbolic expressions.

From (15), (26), (27) and (37), the homogenized in-plane stretch stiffness is given as

$$A_{11}^H = c\langle C_{1111}\rangle = cE_{11}^H$$

where

$$E_{11}^H = 2\int_{0}^{r_2/2}\int_{-1/2}^{1/2} \frac{E_1^{hc2}}{1-\Delta^{[2]}}\left[(1 - v_{23}^{hc2}v_{32}^{hc2})\left(1 + \frac{1}{h_1}\frac{\partial U_1^{[2]}}{\partial y_1}\right) + (v_{31}^{hc2} + v_{21}^{hc2}v_{32}^{hc2})\frac{\partial U_3^{[2]}}{\partial z}\right]\mathrm{d}z\,\mathrm{d}y_1$$

$$+ 2\int_{r_2/2}^{1/2}\int_{-1/2}^{1/2} \frac{E_1^{hc1}}{1-\Delta^{[1]}}\left[(1 - v_{23}^{hc1}v_{32}^{hc1})\left(1 + \frac{1}{h_1}\frac{\partial U_1^{[1]}}{\partial y_1}\right) + (v_{31}^{hc1} + v_{21}^{hc1}v_{32}^{hc1})\frac{\partial U_3^{[1]}}{\partial z}\right]\mathrm{d}z\,\mathrm{d}y_1 \tag{60}$$

And the integration of (60) results

$$E_{11}^{H}=\sum_{n}2(-1)^{n+3/2}\left\{\frac{c_n(v_{31}^{hc1}+v_{21}^{hc1}v_{32}^{hc1})+\left[\frac{2b_n^{[1]}}{n\pi}\sinh(\lambda_n^{[1]}\frac{h_1r_1}{2})-\frac{4}{n^2\pi^2}\right](1-v_{23}^{hc1}v_{32}^{hc1})}{1-\Delta^{[1]}}r_1E_1^{hc1}\right.$$
$$\left.+\frac{c_n(v_{31}^{hc2}+v_{21}^{hc2}v_{32}^{hc2})+\left[\frac{2b_n^{[2]}}{n\pi}\sinh(\lambda_n^{[2]}\frac{h_1r_2}{2})-\frac{4}{n^2\pi^2}\right](1-v_{23}^{hc2}v_{32}^{hc2})}{1-\Delta^{[2]}}r_2E_1^{hc2}\right\}\quad n=1,3,5\ldots \tag{61}$$

Let all the geometrical properties be the same as those of Section 4.2.1 with $r_2=2/3$, then the intermediate equivalent properties expressed by E_1^{hc2} are

$$\begin{aligned}&E_1^{hc2}=\frac{2t_1}{\sqrt{3}b}E_c\\&G_{13}^{hc1}=\frac{1}{5.2}E_1^{hc2}\qquad G_{13}^{hc2}=\frac{1}{2.6}E_1^{hc2}\\&1-\Delta^{[2]}=0.91\end{aligned} \tag{62}$$

and the corresponding terms in (61) are expressed in unit of E_1^{hc2} as

$\frac{t_1}{b}$	0.1	0.05	0.025	0.01
$\frac{(1-v_{32}^{hc1}v_{23}^{hc1})E_1^{hc1}}{1-\Delta^{[1]}}$	0.135833	0.133059	0.132365	0.132171
$\frac{(v_{31}^{hc1}+v_{21}^{hc1}v_{32}^{hc1})E_1^{hc1}}{1-\Delta^{[1]}}$	0.122376	0.122700	0.122781	0.122804
$\frac{(1-v_{32}^{hc1}v_{23}^{hc1})E_3^{hc1}}{1-\Delta^{[1]}}$	2.114191	2.114153	2.114144	2.114144
$\frac{(v_{31}^{hc1}+v_{21}^{hc1}v_{32}^{hc1})E_3^{hc1}}{1-\Delta^{[1]}}$	0.122376	0.122700	0.122781	0.122804

(63)

The substitution of (62) and (63) into (61) results the homogenized stretch stiffness in terms of thickness ratio h_1, and the numerical data are given in Table 2 and shown in Fig. 9.

Remarks

(a) After Becker's (1998) investigation of thickness effect on honeycomb in-plane stiffness, there was no further attention on skin effect on honeycomb sandwich computations. Most of today's sandwich computations follow three-layer theories, where equivalent core properties are obtained without skin effect considered, with existing values corresponding to the LB solution, either implicitly in FEA modeling or explicitly in formulas. As shown in Fig. 10, this may result in stretch stiffness underestimated by about 3–25%

Table 2
Normalized homogenized in-plane stretch stiffness E_{11}^{H}/E_1^{hc2} with $r_2=2/3$

h_1	LB	1/100	1/20	1/10	1/8	1/6	1/5	1/4	1/3	1/2	1	2	10	100	10 000	UB
$t_1/b=0.1$	0.302	0.310	0.313	0.318	0.320	0.324	0.327	0.331	0.340	0.355	0.400	0.484	0.674	0.725	0.732	0.898
$t_1/b=0.05$	0.302	0.304	0.308	0.313	0.315	0.319	0.322	0.324	0.334	0.349	0.496	0.481	0.672	0.725	0.730	0.896
$t_1/b=0.025$	0.302	0.302	0.307	0.311	0.314	0.317	0.321	0.325	0.333	0.348	0.395	0.481	0.672	0.724	0.730	0.896
$t_1/b=0.01$	0.302	0.302	0.306	0.311	0.313	0.317	0.320	0.325	0.333	0.348	0.394	0.480	0.672	0.724	0.730	0.896

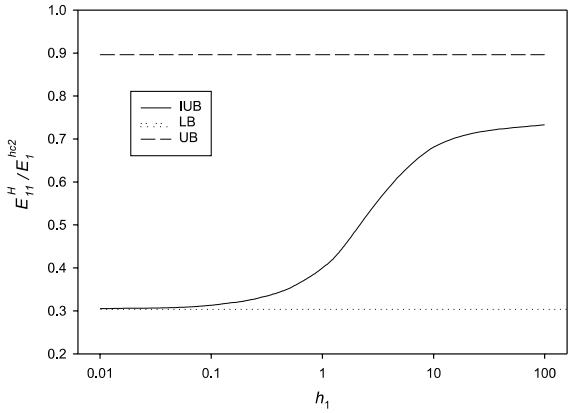

Fig. 9. Stretch stiffness E_{11}^H with $t_1/b = 0.05$.

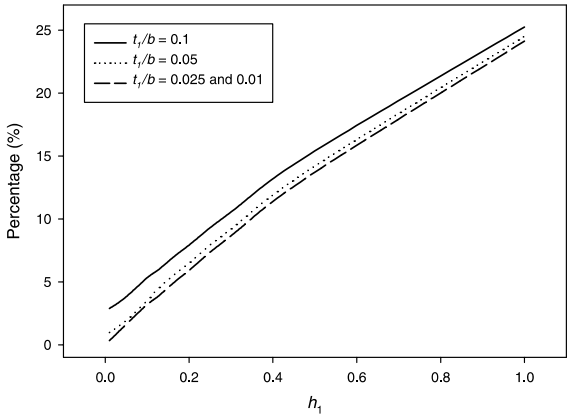

Fig. 10. Underestimation in stretch stiffness E_{11}^H.

when h_1 is increased from 0.1 to 1.0, the range of common honeycomb applications. It is also found that the cell wall thickness ratio t_1/b has little influence on skin effect, particularly when this ratio is less than 0.05.

(b) By applying Reuss model and Voigt model in this case, the formulas for LB and UB are

$$E_{11}^H\big|_{\mathrm{UB}} = r_1\frac{(1-v_{23}^{hc1}v_{32}^{hc1})E_1^{hc1}}{1-\Delta^{[1]}} + r_2\frac{(1-v_{23}^{hc2}v_{32}^{hc2})E_1^{hc2}}{1-\Delta^{[2]}}$$
$$E_{11}^H\big|_{\mathrm{LB}} = \frac{\sigma_1^h}{r_1\left(\frac{\sigma_1^h}{E_1^{hc1}} - v_{21}^{hc1}\frac{\sigma_2^{hc1}}{E_2^{hc1}}\right) + r_2\left(\frac{\sigma_1^h}{E_1^{hc2}} - v_{21}^{hc2}\frac{\sigma_2^{hc2}}{E_2^{hc2}}\right)} \tag{64}$$

Note that to be consistent with the stationary variational principle, in (64) Poisson's effect along z-axis is considered for UB but not for LB (i.e., $\varepsilon_2^h = \varepsilon_3^h = 0$ and $\varepsilon_2^h = \sigma_3^h = 0$ for UB and LB, respectively). The substitution of (34) and (35) into (64) finally results in

$$
\begin{aligned}
E_{11}^H\big|_{\mathrm{UB}} &= \frac{\frac{1}{1-v_c^2}+\frac{2bt_1}{at_2}\cos^4\theta\Phi}{(\cos\theta b/a+1)\sin\theta}(t_2/2b)E_c \\
E_{11}^H\big|_{\mathrm{LB}} &= \frac{(\cos\theta b/a+1)}{\frac{t_2 b\sin\theta}{2t_1 a\cos^2\theta[1+tg^2\theta(t_1/b)^2]}+\sin\theta}(t_2/2b)E_c \\
\Phi_1 &= \frac{1+tg^2\theta(t_1/b)^2[1-\sin^2\theta v_c^2]}{1-\frac{3}{4}v_c^2-\frac{1}{4}v_c^2\cos(4\theta)}
\end{aligned}
\tag{65}
$$

where Poisson's effect is represented by the existence of v_c.

When regular hexagon is considered with parameters $t_2 = 2t_1$, $a = b$, $\theta = 60°$, then for small t_1/b, (65) is approximated as

$$
\begin{aligned}
E_{11}^H\big|_{\mathrm{LB}} &\approx \frac{\sqrt{3}}{5}(t_1/b)E_c \\
E_{11}^H\big|_{\mathrm{UB}} &\approx \frac{\sqrt{3}}{2(1-v_c^2)}(t_1/b)E_c
\end{aligned}
\tag{66}
$$

which agree with the results of $(\sqrt{3}/5)(t_1/b)E_c$ given by Shi and Tong (1995b) and Becker (1998); whereas the formula of Parton and Kudryavtsev (1993) seems to overestimate stretch stiffness.

The formula (61) is an IUB because the skin faces are assumed infinite rigid. Note the strain is allowed in three direction so that the derivation is consistent with real situations such as in compression buckling. It can be seen that, when $h_1 \to 0$, the IUB of this study converge to the LB in (65) when cell wall thickness ratio is not higher than 0.025. The IUB does not converge to the UB of (65) when $h_1 \to \infty$ because the UB formula in (65) assumes zero strain in three direction.

(c) The homogenized in-plane stiffness E_{21}^H is readily obtainable with the same displacement field (54)

$$A_{21}^H = c\langle C_{2211}\rangle = cE_{21}^H$$

where

$$
\begin{aligned}
E_{21}^H = {} & 2\int_0^{r_2/2}\int_{-1/2}^{1/2}\frac{E_2^{hc2}}{1-\Delta^{[2]}}\left[(v_{12}^{hc2}+v_{13}^{hc2}v_{32}^{hc2})\left(1+\frac{1}{h_1}\frac{\partial U_1^{[2]}}{\partial y_1}\right)+(v_{32}^{hc2}+v_{12}^{hc2}v_{31}^{hc2})\frac{\partial U_3^{[2]}}{\partial z}\right]\mathrm{d}z\,\mathrm{d}y_1 \\
& + 2\int_{r_2/2}^{1/2}\int_{-1/2}^{1/2}\frac{E_2^{hc1}}{1-\Delta^{[1]}}\left[(v_{12}^{hc1}+v_{13}^{hc1}v_{32}^{hc1})\left(1+\frac{1}{h_1}\frac{\partial U_1^{[1]}}{\partial y_1}\right)+(v_{32}^{hc1}+v_{12}^{hc1}v_{31}^{hc1})\frac{\partial U_3^{[1]}}{\partial z}\right]\mathrm{d}z\,\mathrm{d}y_1
\end{aligned}
\tag{67}
$$

By considering $E_2^{hc2} = 0$ in (34), the integration of (67) results

$$
\begin{aligned}
E_{21}^H &= \sum_n 2(-1)^{n+3/2}\frac{c_n(v_{32}^{hc1}+v_{12}^{hc1}v_{31}^{hc1})+\left[\frac{2b_n^{[1]}}{n\pi}\sinh\left(\lambda_n^{[1]}\frac{h_1 r_1}{2}\right)-\frac{4}{n^2\pi^2}\right](v_{12}^{hc1}+v_{13}^{hc1}v_{32}^{hc1})}{1-\Delta^{[1]}}r_1 E_2^{hc1} \\
n &= 1,3,5,\ldots
\end{aligned}
\tag{68}
$$

The eigenvalues and coefficients in (68) are the same as those of (61).

In converse to the case of E_{11}^H, the formula (68) is an Improved Lower Bound (ILB) with the assumption of infinite rigid skin faces, which is also noted by Hohe and Becker (2001). The numerical results are omitted here.

(d) Similar to the case of G_{23}^H, from the GTM in Section 4.1, the third homogenized in-plane stiffness E_{22}^H can be easily derived with parallel model or Reuss model by considering $\varepsilon_3^h = 0$

$$E_{22}^H = r_1(1-v_{13}^{hc1}v_{31}^{hc1})\frac{E_2^{hc1}}{1-\Delta^{[1]}}+r_2(1-v_{13}^{hc2}v_{31}^{hc2})\frac{E_2^{hc2}}{1-\Delta^{[2]}} \tag{69}$$

And the substitution of (34) and (35) into (69) finally gives

$$E_{22}^{H} = \frac{\sin^3\theta\Phi_2}{\cos\theta + a/b}(t_1/b)E_c$$
$$\Phi_2 = \frac{1 + (t_1/b)^2[\csc\theta\, ctg^2\theta - v_c^2\cos^2\theta\csc^2\theta]}{1 - \frac{3}{4}v_c^2 - \frac{1}{4}v_c^2\cos(4\theta)} \tag{70}$$

For regular hexagons with $t_2 = 2t_1$, $a = b$, $\theta = 60^\circ$ and small t_1/b, (70) is approximated as

$$E_{22}^{H} \approx \frac{\sqrt{3}}{4\left(1 - \frac{5}{8}v_c^2\right)}(t_1/b)E_c \tag{71}$$

The real value of E_{22}^{H} should be under between zero and full Poisson's effect, i.e., between $(\sqrt{3}/4)(t_1/b)E_c$ and $(\sqrt{3}/4(1 - \frac{5}{8}v_c^2))(t_1/b)E_c$. Compared with (66) it can be found that the stretch stiffness of regular honeycomb structures becomes a little anisotropic due to skin effect.

(e) The unit width stretch stiffness of a honeycomb sandwich thus can be calculated with

$$A_{11} = cE_{11}^{H} + 2t_{\mathrm{f}}\frac{E_{\mathrm{f}}}{1 - v_{\mathrm{f}}^2}$$
$$A_{22} = cE_{22}^{H} + 2t_{\mathrm{f}}\frac{E_{\mathrm{f}}}{1 - v_{\mathrm{f}}^2} \tag{72}$$
$$A_{21} = cE_{21}^{H} + 2t_{\mathrm{f}}\frac{v_{\mathrm{f}}E_{\mathrm{f}}}{1 - v_{\mathrm{f}}^2}$$

4.2.3. Homogenized flexural stiffness

Similar to Sections 4.2.1 and 4.2.2, from (32) the governing equations of cylindrical bending are given below

$$G_{13}^{hc\alpha}\left(\frac{\partial^2 V_1^{[\alpha]}}{\partial z^2} + \frac{1}{h_1}\frac{\partial^2 V_3^{[\alpha]}}{\partial y_1\partial z}\right) + \frac{E_1^{hc\alpha}}{1 - \Delta^{[\alpha]}}\left[(v_{31}^{hc\alpha} + v_{21}^{hc\alpha}v_{32}^{hc\alpha})\frac{1}{h_1}\frac{\partial^2 V_3^{[\alpha]}}{\partial y_1\partial z} + (1 - v_{32}^{hc\alpha}v_{23}^{hc\alpha})\frac{1}{h_1^2}\frac{\partial^2 V_1^{[\alpha]}}{\partial y_1^2}\right] = 0$$
$$G_{13}^{hc\alpha}\left(\frac{1}{h_1}\frac{\partial^2 V_1^{[\alpha]}}{\partial y_1\partial z} + \frac{1}{h_1^2}\frac{\partial^2 V_3^{[\alpha]}}{\partial y_1^2}\right) + \frac{E_3^{hc\alpha}}{1 - \Delta^{[\alpha]}}\left[(v_{13}^{hc\alpha} + v_{12}^{hc\alpha}v_{23}^{hc\alpha})\frac{1}{h_1}\frac{\partial^2 V_1^{[\alpha]}}{\partial y_1\partial z} + (1 - v_{12}^{hc\alpha}v_{21}^{hc\alpha})\frac{\partial^2 V_3^{[\alpha]}}{\partial z^2}\right] = 0 \tag{73}$$
$$\Delta^{[\alpha]} = v_{12}^{hc\alpha}v_{21}^{hc\alpha} + v_{13}^{hc\alpha}v_{31}^{hc\alpha} + v_{23}^{hc\alpha}v_{32}^{hc\alpha} + v_{12}^{hc\alpha}v_{23}^{hc\alpha}v_{31}^{hc\alpha} + v_{13}^{hc\alpha}v_{21}^{hc\alpha}v_{32}^{hc\alpha}$$

Based on the symmetry of material and loading about z-axis, and the anti-symmetry of loading about y_1-axis, the displacement field is constructed as

$$V_1^{[1]} = \sum_n d_n^{[1]}\sinh\left[\lambda_n^{[1]}h_1\left(y_1 - \frac{1}{2}\right)\right]\sin(n\pi z), \quad n = 2,4,6\ldots$$
$$V_3^{[1]} = \frac{1}{2}v_{13}^{hc1}z^2 + \sum_n f_n\cos(n\pi z), \quad n = 2,4,6\ldots$$
$$V_1^{[2]} = \sum_n d_n^{[2]}\sinh\left(\lambda_n^{[2]}h_1y_1\right)\sin(n\pi z), \quad n = 2,4,6\ldots \tag{74}$$
$$V_3^{[2]} = \frac{1}{2}v_{13}^{hc2}z^2 + \sum_n f_n\cos(n\pi z), \quad n = 2,4,6\ldots$$

Note that in (74) the first term of V_3 expression is added to ensure displacement continuity. As the equilibrium condition along y_1-axis is more important than that along z-axis, (74) is substituted into the first equation of (73) to obtain eigenvalues

$$\lambda_n^{[1]} = n\pi\sqrt{\frac{G_{13}^{hc1}(1-\Delta^{[1]})}{E_1^{hc1}(1-\nu_{23}^{hc1}\nu_{32}^{hc1})}}$$
$$\lambda_n^{[2]} = n\pi\sqrt{\frac{G_{13}^{hc2}(1-\Delta^{[2]})}{E_1^{hc2}(1-\nu_{23}^{hc2}\nu_{32}^{hc2})}} \tag{75}$$

The solutions of three unknown coefficients in (74) are just similar to those presented in Section 4.2.2 by the Rayleigh–Ritz Method. The expression of strain energy is given below, whilst the symbolic calculation and the expressions of d_n and f_n are omitted here.

$$I(V) = Q_s + Q_y + Q_z$$

$$Q_s = 2\int_{-1/2}^{1/2}\int_0^{r_2/2}\frac{1}{2}G_{13}^{hc2}\left(\frac{\partial V_1^{[2]}}{\partial z}+\frac{1}{h_1}\frac{\partial V_3^{[2]}}{\partial y_1}\right)^2 \mathrm{d}y_1\,\mathrm{d}z + 2\int_{-1/2}^{1/2}\int_{r_2/2}^{1/2}\frac{1}{2}G_{13}^{hc1}\left(\frac{\partial V_1^{[1]}}{\partial z}+\frac{1}{h_1}\frac{\partial V_3^{[1]}}{\partial y_1}\right)^2 \mathrm{d}y_1\,\mathrm{d}z$$

$$Q_y = 2\int_{-1/2}^{1/2}\int_0^{r_2/2}\frac{1}{2}\frac{E_1^{hc2}}{1-\Delta^{[2]}}\left[(\nu_{31}^{hc2}+\nu_{21}^{hc2}\nu_{32}^{hc2})\frac{\partial V_3^{[2]}}{\partial z}+(1-\nu_{32}^{hc2}\nu_{23}^{hc2})\left(\frac{1}{h_1}\frac{\partial V_1^{[2]}}{\partial y_1}+z\right)\right]\left(\frac{1}{h_1}\frac{\partial V_1^{[2]}}{\partial y_1}+z\right)\mathrm{d}y_1\,\mathrm{d}z$$
$$+ 2\int_{-1/2}^{1/2}\int_{r_2/2}^{1/2}\frac{1}{2}\frac{E_1^{hc1}}{1-\Delta^{[1]}}\left[(\nu_{31}^{hc1}+\nu_{21}^{hc1}\nu_{32}^{hc1})\frac{\partial V_3^{[1]}}{\partial z}+(1-\nu_{32}^{hc1}\nu_{23}^{hc1})\left(\frac{1}{h_1}\frac{\partial V_1^{[1]}}{\partial y_1}+z\right)\right]\left(\frac{1}{h_1}\frac{\partial V_1^{[1]}}{\partial y_1}+z\right)\mathrm{d}y_1\,\mathrm{d}z$$

$$Q_z = 2\int_{-1/2}^{1/2}\int_0^{r_2/2}\frac{1}{2}\frac{E_3^{hc2}}{1-\Delta^{[2]}}\left\{(\nu_{13}^{hc2}+\nu_{13}^{hc2}\nu_{23}^{hc2})\left(\frac{1}{h_1}\frac{\partial V_1^{[2]}}{\partial y_1}+z\right)+\left[\frac{\partial V_3^{[2]}}{\partial z}-(\nu_{13}^{hc2}+\nu_{12}^{hc2}\nu_{23}^{hc2})z\right](1-\nu_{12}^{hc2}\nu_{21}^{hc2})\right\}$$
$$\times\left[\frac{\partial V_3^{[2]}}{\partial z}-(\nu_{13}^{hc2}+\nu_{12}^{hc2}\nu_{23}^{hc2})z\right]\mathrm{d}y_1\,\mathrm{d}z + 2\int_{-1/2}^{1/2}\int_{r_2/2}^{1/2}\frac{1}{2}\frac{E_3^{hc1}}{1-\Delta^{[1]}}\left\{(\nu_{13}^{hc1}+\nu_{13}^{hc1}\nu_{23}^{hc1})\left(\frac{1}{h_1}\frac{\partial V_1^{[1]}}{\partial y_1}+z\right)\right.$$
$$\left.+\left[\frac{\partial V_3^{[1]}}{\partial z}-(\nu_{13}^{hc1}+\nu_{12}^{hc1}\nu_{23}^{hc1})z\right](1-\nu_{12}^{hc1}\nu_{21}^{hc1})\right\}\left[\frac{\partial V_3^{[1]}}{\partial z}-(\nu_{13}^{hc1}+\nu_{12}^{hc1}\nu_{23}^{hc1})z\right]\mathrm{d}y_1\,\mathrm{d}z \tag{76}$$

From (15), (26), (27) and (37), we can have homogenized flexural stiffness as

$$D_{11}^H = c^3\langle C_{1111}^*\rangle = \frac{c^3}{12}E_{11}^{*H}$$

where

$$E_{11}^{*H} = 12\times\left\{2\int_0^{r_2/2}\int_{-1/2}^{1/2}\frac{E_1^{hc2}}{1-\Delta^{[2]}}\left[(1-\nu_{23}^{hc2}\nu_{32}^{hc2})\left(z^2+z\frac{1}{h_1}\frac{\partial V_1^{[2]}}{\partial y_1}\right)+z(\nu_{31}^{hc2}+\nu_{21}^{hc2}\nu_{32}^{hc2})\frac{\partial V_3^{[2]}}{\partial z}\right]\mathrm{d}z\,\mathrm{d}y_1\right.$$
$$\left.+2\int_{r_2/2}^{1/2}\int_{-1/2}^{1/2}\frac{E_1^{hc1}}{1-\Delta^{[1]}}\left[(1-\nu_{23}^{hc1}\nu_{32}^{hc1})\left(z^2+z\frac{1}{h_1}\frac{\partial V_1^{[1]}}{\partial y_1}\right)+z(\nu_{31}^{hc1}+\nu_{21}^{hc1}\nu_{32}^{hc1})\frac{\partial V_3^{[1]}}{\partial z}\right]\mathrm{d}z\,\mathrm{d}y_1\right\} \tag{77}$$

The integration of (77) results

$$E_{11}^{*H} = 12 \times \sum_n (-1)^{\frac{n}{2}} \left\{ \frac{r_1 f_n (v_{31}^{hc1} + v_{21}^{hc1} v_{32}^{hc1}) - \left[\frac{2d_n^{[1]}}{h_1 n\pi} \sinh\left(\lambda_n^{[1]} \frac{h_1 r_1}{2}\right) + \frac{2(-1)^{\frac{n}{2}} r_1}{n^2\pi^2} \right] (1 - v_{23}^{hc1} v_{32}^{hc1})}{1 - \Delta^{[1]}} E_1^{hc1} \right.$$
$$\left. + \frac{r_2 f_n (v_{31}^{hc2} + v_{21}^{hc2} v_{32}^{hc2}) - \left[\frac{2d_n^{[2]}}{h_1 n\pi} \sinh\left(\lambda_n^{[2]} \frac{h_1 r_2}{2}\right) + \frac{2(-1)^{\frac{n}{2}} r_2}{n^2\pi^2} \right] (1 - v_{23}^{hc1} v_{32}^{hc1})}{1 - \Delta^{[2]}} E_1^{hc2} \right\} \quad n = 2, 4, 6 \ldots \tag{78}$$

The alternative way is to use the form of energy equivalence $\langle E_{11}^{*H} \rangle = 12 \times 2 \times I(V)$.

With the hexagon configuration data as before, the numerical results for the flexural stiffness are given in Table 3 and shown in Fig. 11.

Remarks

(a) In the present study, this is the first attempt where the flexural stiffness is distinguished from the stretch stiffness, i.e., $E_{11}^{*H} \neq E_{11}^{H}$. The difference can be as high as 25% for the case $h_1 = 1$, as shown in Fig. 12. It is interesting to note that when $h_1 \to 0$ or ∞, the two stiffness converge to each other.

Most current sandwich computational approaches have questionable approximations in the continuum modeling of honeycomb core because skin effect has never been taken into account. For regular hexagons as shown in Fig. 13, the flexural stiffness is 5–40% underestimated when h_1 increases from 0.05 to 1.0. The consequence of the errors has to be evaluated in particular cases; however, it is suggested that all computational modeling use the corrected homogenized properties since the required efforts are minimum.

Table 3
Normalized homogenized flexural stiffness E_{11}^{*H}/E_1^{hc2} with $r_2 = 2/3$

h_1	LB	1/10 000	1/100	1/20	1/10	1/8	1/6	1/5	1/4	1/3	1/2	1	2	10	100	10 000	UB
$t_1/b = 0.1$	0.304	0.308	0.310	0.320	0.334	0.340	0.351	0.359	0.371	0.391	0.427	0.514	0.608	0.705	0.727	0.730	0.898
$t_1/b = 0.05$	0.302	0.303	0.305	0.315	0.329	0.335	0.346	0.354	0.367	0.386	0.423	0.511	0.606	0.704	0.726	0.729	0.896
$t_1/b = 0.025$	0.300	0.301	0.303	0.314	0.327	0.334	0.345	0.353	0.366	0.385	0.422	0.510	0.605	0.704	0.726	0.728	0.896
$t_1/b = 0.01$	0.300	0.301	0.303	0.314	0.327	0.334	0.345	0.353	0.366	0.385	0.422	0.510	0.605	0.704	0.726	0.728	0.896

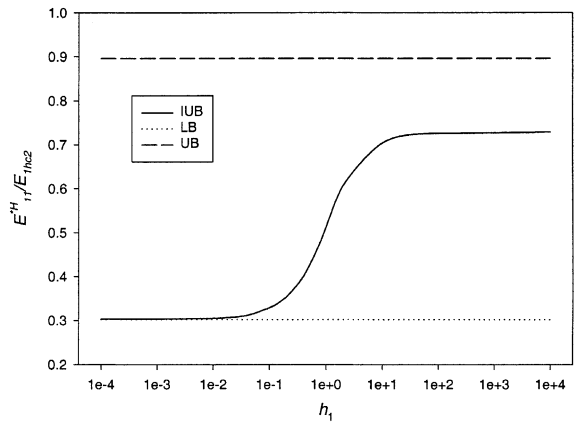

Fig. 11. Flexural stiffness E_{11}^{*H} with $t_1/b = 0.05$.

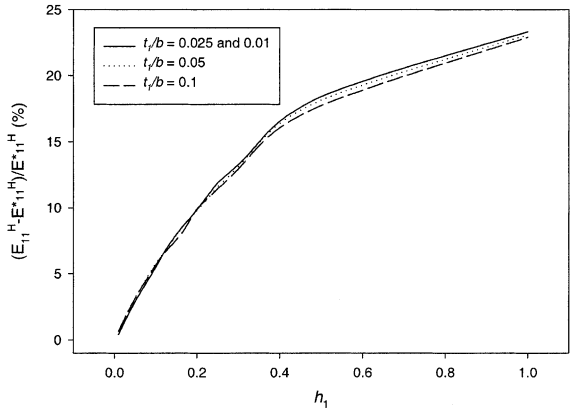

Fig. 12. Percentage difference between stretch and flexural stiffness.

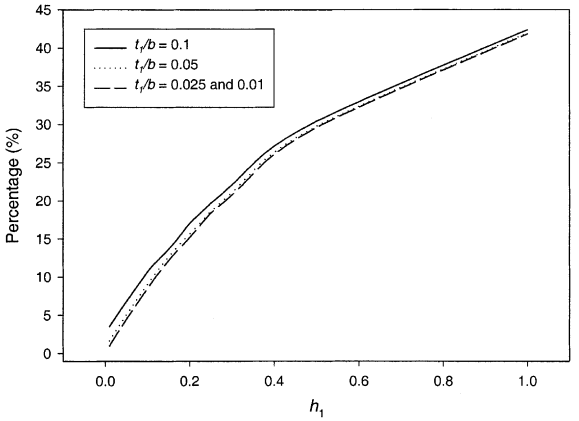

Fig. 13. Underestimation in flexural stiffness E_{11}^{*H}.

(b) The formula of the panel unit width cylindrical flexural rigidity is

$$\begin{aligned} D_{11} &= \frac{c^3}{12}E_{11}^{*H} + \frac{(t_f+c)^2 t_f}{2}\frac{E_f}{1-v_f^2} + \frac{t_f^3}{12}\frac{E_f}{1-v_f^2} \\ D_{22} &= \frac{c^3}{12}E_{22}^{*H} + \frac{(t_f+c)^2 t_f}{2}\frac{E_f}{1-v_f^2} + \frac{t_f^3}{12}\frac{E_f}{1-v_f^2} \\ D_{21} &= \frac{c^3}{12}E_{21}^{*H} + \frac{(t_f+c)^2 t_f}{2}\frac{v_f E_f}{1-v_f^2} + \frac{t_f^3}{12}\frac{v_f E_f}{1-v_f^2} \end{aligned} \tag{79}$$

When t_1/b increases from 0.01 to 0.1, the hexagon core can have more than 20% contribution in total flexural rigidity if $c/t_f = 50$. The anti-plane assumption thus should be carefully used in computations of honeycomb sandwiches. By using equivalent anti-plane assumption, core shear stiffness was defined by Allen (1969) as

$$G_{13}^{*H} = \frac{G_{13}^{H}}{1 + \frac{E_{11}^{*H}\left(1-v_f^2\right)}{6E_f}\frac{c^2}{t_f(c+t_f)}} \tag{80}$$

It is found that the transverse shear stiffness can be much overestimated by ignoring the core's flexural stiffness. This may partially explain the long existing contradiction that shear stiffness obtained from testing is always larger than theoretical UB, especially for three point bending testing where shear stiffness is highly sensitive to the accuracy of flexural rigidity.

(c) Following a similar derivation, the flexural stiffness E_{21}^{*H} is given below

$$D_{21}^{H} = c^3\langle C_{2211}^{*}\rangle = \frac{\delta^3}{12}E_{21}^{*H}$$

where

$$E_{21}^{*H} = 12\times\left\{2\int_0^{r_2/2}\int_{-1/2}^{1/2}\frac{E_1^{hc2}}{1-\Delta^{[2]}}\left[(v_{12}^{hc2}+v_{13}^{hc2}v_{32}^{hc2})\left(z^2+z\frac{1}{h_1}\frac{\partial V_1^{[2]}}{\partial y_1}\right)+z(v_{32}^{hc2}+v_{12}^{hc2}v_{31}^{hc2})\frac{\partial V_3^{[2]}}{\partial z}\right]\mathrm{d}z\,\mathrm{d}y_1\right.$$
$$\left.+2\int_{r_2/2}^{1/2}\int_{-1/2}^{1/2}\frac{E_1^{hc1}}{1-\Delta^{[1]}}\left[(v_{12}^{hc1}+v_{13}^{hc1}v_{32}^{hc1})\left(z^2+z\frac{1}{h_1}\frac{\partial V_1^{[1]}}{\partial y_1}\right)+z(v_{32}^{hc1}+v_{12}^{hc1}v_{31}^{hc1})\frac{\partial V_3^{[1]}}{\partial z}\right]\mathrm{d}z\,\mathrm{d}y_1\right\} \tag{81}$$

and the integration of which results in

$$E_{21}^{*H} = 12\times\sum_n(-1)^{\frac{n}{2}}\frac{r_1 f_n(v_{32}^{hc1}+v_{12}^{hc1}v_{31}^{hc1})-\left[\frac{2d_n^{[1]}}{h_1 n\pi}\sinh(\lambda_n^{[1]}\frac{h_1 r_1}{2})+\frac{2(-1)^{\frac{n}{2}}r_1}{n^2\pi^2}\right](v_{12}^{hc1}+v_{13}^{hc1}v_{32}^{hc1})}{1-\Delta^{[1]}}E_1^{hc1}$$
$$n=2,4,6\ldots \tag{82}$$

since $E_2^{hc2}\approx 0$.

For the case of E_{22}^{*H}, as seen from the GTM in Fig. 5, the only skin effect is due to Poisson's effect. Therefore its value is the same as E_{22}^{H} per Eq. (70), i.e.,

$$E_{22}^{*H} = E_{22}^{H} \tag{83}$$

5. Periodic unit cell finite element analysis

5.1. Periodic boundary conditions

To verify the variational approach given in the preceding section, the method of unit cell FEA (Xu, 2001) is used, which is much more effective than actual detailed modeling in terms of computations and the obviation of size and edge effects. Besides the verification of IUB of semi-analytical solutions in Section 4, the unit cell FEA can further demonstrate the effect of skin rigidity on the homogenized properties, by which Eqs. (91) and (92) and the correction coefficients which are later shown in Table 7 are proposed.

The technique of unit cell modeling is on how to impose periodic boundary conditions in both displacement and stress fields; whereas most FEA homogenization problems have to be treated with specialized hybrid elements. In this study with common elements of commercial FEA program (ANSYS5.5), a unit cell modeling technique is developed, due to the transverse symmetry of sandwiches.

First the stress function Ψ is introduced by

$$\sigma_y = \frac{\partial^2\Psi}{\partial z^2}\qquad \sigma_z = \frac{\partial^2\Psi}{\partial y^2}\qquad \tau_{zy} = -\frac{\partial^2\Psi}{\partial y\,\partial z} \tag{84}$$

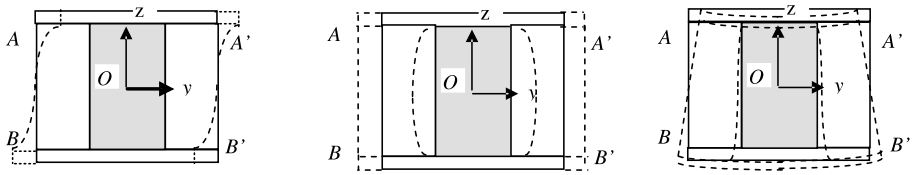

Fig. 14. Deformation of periodic unit cell in (a) shear, (b) tension and (c) bending.

In Fig. 14, the displacement and stress are continuous with regard to the boundary AB and $A'B'$, i.e.,

$$\begin{aligned} &\sigma_1^h\left(-\frac{1}{2},z\right)=\sigma_1^h\left(\frac{1}{2},z\right) \qquad \tau_{13}^h\left(-\frac{1}{2},z\right)=\tau_{13}^h\left(\frac{1}{2},z\right)\\ &\Theta_1\left(-\frac{1}{2},z\right)=\Theta_1\left(\frac{1}{2},z\right) \qquad \Theta_3\left(-\frac{1}{2},z\right)=\Theta_3\left(\frac{1}{2},z\right) \end{aligned} \tag{85}$$

where Θ represents the homogenization function Π, U or V for the mode of shear, tension and bending, respectively.

5.1.1. Pure transverse shear mode

In the case of transverse shear mode, clearly there is an anti-symmetric relation between AB and $A'B'$, i.e.,

$$\begin{aligned} &\sigma_1^h\left(-\frac{1}{2},z\right)=\sigma_1^h\left(\frac{1}{2},-z\right) \qquad \tau_{13}^h\left(-\frac{1}{2},z\right)=\tau_{13}^h\left(\frac{1}{2},-z\right)\\ &\Pi_1\left(-\frac{1}{2},z\right)=-\Pi_1\left(\frac{1}{2},-z\right) \qquad \Pi_3\left(-\frac{1}{2},z\right)=-\Pi_3\left(\frac{1}{2},-z\right) \end{aligned} \tag{86}$$

From (84)–(86) it is found that $(\partial^2\Psi/\partial z^2)(\pm\frac{1}{2},z)$, $(\partial^2\Psi/\partial y^2)(\pm\frac{1}{2},z)$ and $(\partial^2\Psi/\partial y\partial z)(\pm\frac{1}{2},z)$ are all even about z. The followings thus can be deduced sequentially,

$$\begin{aligned} &\sigma_1^h\left(\pm\frac{1}{2},z\right)=\sigma_3^h\left(\pm\frac{1}{2},z\right)=0\\ &\varepsilon_1^h\left(\pm\frac{1}{2},z\right)=\varepsilon_3^h\left(\pm\frac{1}{2},z\right)=0 \end{aligned} \tag{87}$$

By (87) the periodic boundary condition for FEA modeling can be finally defined in the form of

$$\Pi_3\left(\pm\frac{1}{2},z\right)=\Pi_3(0,z)=0 \tag{88}$$

5.1.2. Pure tension and bending mode

With similar deduction, the periodic boundary conditions for tension and bending model are, respectively, given as

$$U_1\left(\pm\frac{1}{2},z\right)=U_1(0,z)=0 \tag{89}$$

and

$$V_1\left(\pm\frac{1}{2},z\right)=V_1(0,z)=0 \tag{90}$$

The deformations of the three modes are illustrated by dashed line in Fig. 14.

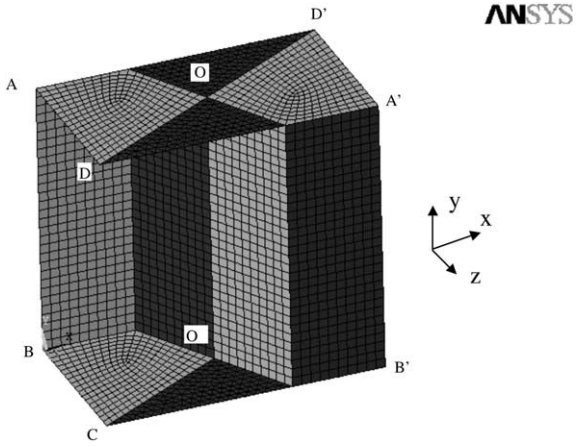

Fig. 15. Unit cell FE modeling.

Table 4
Boundary conditions of periodic unit cell FE modeling

Mode	Nodes	UX	UY	UZ	ROTX	ROTY	ROTZ	Remark
Transverse shear	A′B′CD/ ABC′D′	F	F	0	0	0	F	sym.
	AD/A′D′	$+\Delta$	0	0	F	0	0	
	BC/B′C′	$-\Delta$	0	0	F	0	0	
	AB/OO′/ A′B′	F	0	0	0	0	F	
	DOD′/ CO′C′	F	0	0	F	F	F	add.
In-plane tension	A′B′CD/ ABC′D′	F	F	0	0	0	F	sym.
	AD/BC/AB	$-\Delta$	F	F	F	0	0	
	A′D′/B′C′/ A′B′	$+\Delta$	F	F	F	0	0	
Cylindrical bending	A′B′CD/ ABC′D′	F	F	0	0	0	F	sym.
	AD	$+\Delta$	F	F	F	0	$-2\Delta/(t_f+\delta)$	
	BC	$-\Delta$	F	F	F	0	$-2\Delta/(t_f+\delta)$	
	A′D′	$-\Delta$	F	F	F	0	$+2\Delta/(t_f+\delta)$	
	B′C′	$+\Delta$	F	F	F	0	$+2\Delta/(t_f+\delta)$	
	AB	L	F	0	0	0	$-2\Delta/(t_f+\delta)$	
	A′B′	L	F	0	0	0	$+2\Delta/(t_f+\delta)$	

Note: F—free; L—linear.

5.2. Three-dimensional modeling and results

With the deduction of 2-D periodic boundary conditions in Section 5.1, actual hexagons can be modeled by extending 2-D conditions to 3-D ones. As shown in Fig. 15, there are two periodic sections $ABCD$ and $A'B'C'D'$, and the displacement constraints are imposed as listed in Table 4. For all three modes, plane strain globally occurs in x–y plane, i.e., no displacement in z for two lateral cell walls. In the transverse shear mode, the nodes at the lines $DOD'/CO'C'$ have zero displacement in UY and UZ due to double symmetry, which is additionally imposed to ensure the accuracy of the modeling.

SHELL ELEMENT 93 in ANSYS 5.5 is used for the modeling of core walls and skin faces. The refinement study indicates that the convergence can be quickly achieved, and the final mesh is illustrated in Fig. 15 for the case of $h_1 = 1$.

5.2.1. Non-linear effect

To the authors' knowledge, the non-linear effect, mainly due to membrane force of skin faces, is by this study first time assessed. The assessment is conducted for three modes separately, though not the combination of them. It is observed that the nonlinear effect becomes more evident with the increased ratio $R_n = t_f E_f / cE_c$, and the nonlinear cases are modeled to assess the sensitivity of the ratio R_n. As shown in Table 5, for the case of $R_n = 5/3$ and shear strain up to $1000\mu\varepsilon$, the resulting difference of G_{13}^H is less than 0.08%. Since the ratio R_n of practical applications is mostly less than 0.1, the nonlinear effect can be overlooked particularly in elastic range, and is not considered in this study.

5.2.2. Transverse shear stiffness

It may be reasonable that the effect of skin rigidity can be expressed by the skin rigidity ratio $(t_f/c)^3 E_f / \left| G_{13}^{hc1} - G_{13}^{hc1} \right|$, and an approximate Eq. (91) is thus developed by interpolating of groups of FEA results for G_{13}^H of regular hexagons, which complements IUB solution of (46),

Table 5
Non-linear effect on G_{13}^H / G_{13}^{hc1}

	Shear strain ($R_n = 5/3$)					
	$100\mu\varepsilon$	$200\mu\varepsilon$	$350\mu\varepsilon$	$575\mu\varepsilon$	$925\mu\varepsilon$	$1000\mu\varepsilon$
Non-linear	1.5844	1.5844	1.5845	1.5849	1.5845	1.5846
Linear	1.5836	1.5836	1.5836	1.5836	1.5836	1.5836

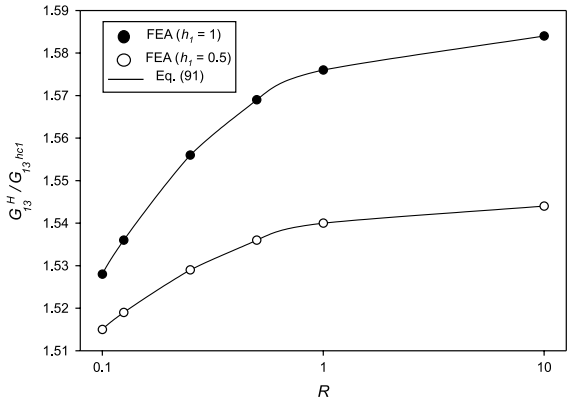

Fig. 16. Effect of skin rigidity: Eq. (91) vs. FEA.

$$G_{13}^{H} = G_{13}^{H}\big|_{\mathrm{IUB}} - \frac{h_1}{120}R^{-5/6}, \quad R \geqslant 0.1$$
$$R = 0.54\left(\frac{t_f}{c}\right)^3 \frac{b}{t_1}\frac{E_f}{E_c} \tag{91}$$

Table 6
G_{13}^{H}/G_{13}^{hc1}: Eq. (91) vs. FEA results

	R					
	0.1	0.125	0.25	0.5	1	10
$h_1 = 1$						
Eq. (91)	1.527	1.537	1.558	1.569	1.576	1.583
FEA	1.528	1.536	1.556	1.569	1.576	1.584
$h_1 = 1/2$						
Eq. (91)	1.516	1.521	1.531	1.537	1.540	1.543
FEA	1.516	1.520	1.531	1.537	1.540	1.544
$h_1 = 1/4$						
Eq. (91)	1.507	1.509	1.514	1.517	1.519	1.521
FEA	1.506	–	–	–	1.519	1.521

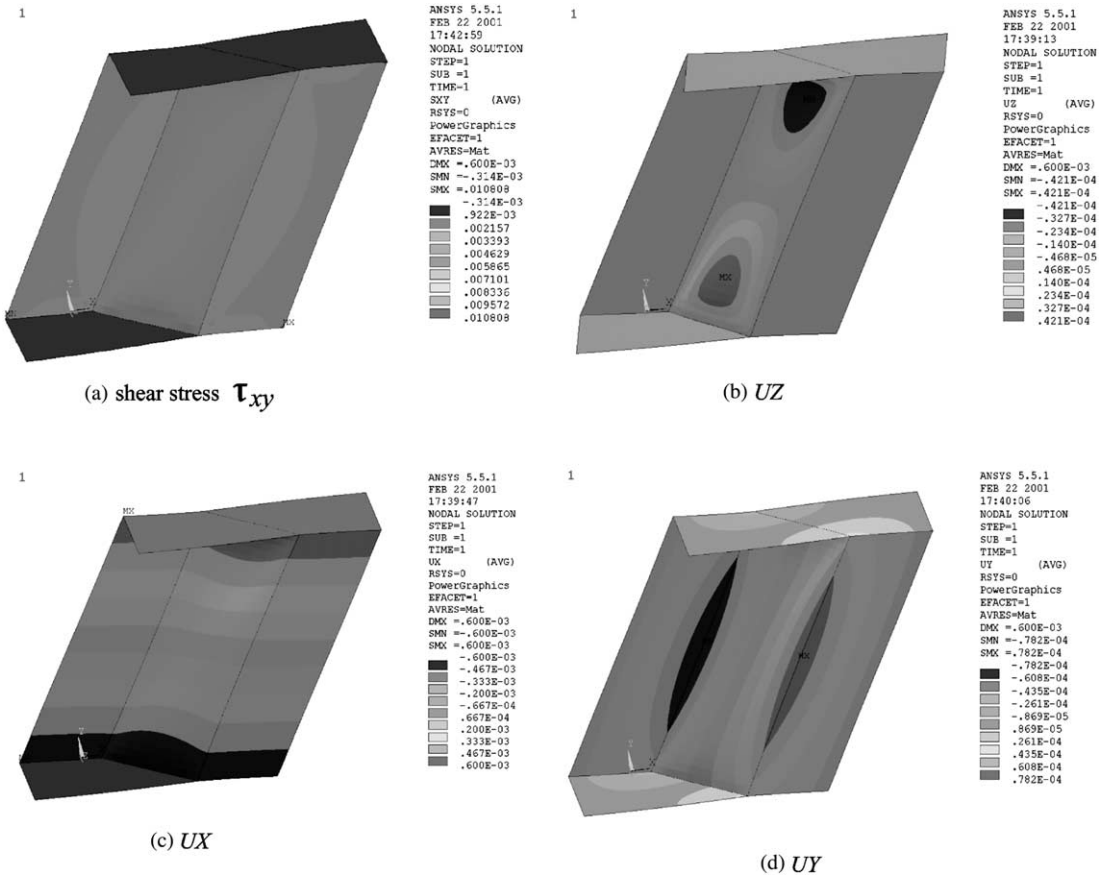

Fig. 17. Pure transverse shear mode.

where $G_{13}^{H}|_{\mathrm{IUB}}$ is calculated by (46), and listed in Table 1. For those hexagons $R < 0.1$, the G_{13}^{H} value can approximately take the LB value of Eq. (49). Eq. (91) is validated for those of $h_1 < 1$, the range of which is sufficient for general honeycomb sandwiches. Further note for anisotropic skin faces, E_{f} in (91) can be approximately replaced with E_{f1}. The closeness of (91) to FEA results is shown in Fig. 16 and Table 6 with less than 1/750 of difference. The deformations of the unit cell shear are illustrated in Fig. 17.

5.2.3. Tension and flexural stiffness

The formulas (61) and (77) developed in Section 4 for tension and flexural stiffness are based on the assumption of infinite rigid skin faces, which result in the IUB. In this study, by using FEA, the effect of skin rigidity can be further assessed and is expressed by two correction coefficients K and K^* for tension and flexural stiffness, respectively.

$$\begin{aligned} E_{11}^{H} &= K E_{11}^{H}\big|_{\mathrm{IUB}} \\ E_{11}^{*H} &= K^* E_{11}^{*H}\big|_{\mathrm{IUB}} \end{aligned} \tag{92}$$

The correction coefficients are listed in Table 7 with respect to the ratios of t_1/b, E_{f}/E_c, and t_{f}/c that cover most of common sandwiches. It is found that when $h_1 < 1/8$ and 1/4, respectively, the correction coefficients K and K^* can be approximated to be 1.00. For the higher value of h_1, the correction coefficients in Table 7 can be used in combination with (61) or (77) to include the rigidity of skin faces. The deformations of tension and bending are illustrated in Figs. 18 and 19.

Table 7
Correction coefficients K and K^*

t_1/b	E_{f}/E_c	t_{f}/δ	K	K^*
$h_1 = 1$				
0.1	1–2	1/12	0.86–0.90	0.93–0.94
	1–2	1/6	0.91–0.93	
	Others	1–2	1/60–1/24	0.86–0.91
0.90–0.93		1–2	1/12–1/6	0.91–0.92
0.94–0.97	*$h_1 = 1/2$*			
0.1	1	1/24–1/12	0.88–0.91	0.94–0.96
	2	1/12–1/6	0.93–0.95	0.97–0.99
Others	1–2	1/24–1/6	0.91–0.92	0.97–0.99
$h_1 = 1/4$				
0.1	1–2	1/48–1/24	0.89–0.91	0.97–1.00
		1/12–1/6	0.92–0.94	
	Others	1	1/120–1/24	0.89–0.91
0.97–0.99		2	1/24–1/6	0.91–0.93
0.99–1.00	*$h_1 = 1/5$*			
0.1	1–2	1/60–1/6	0.91–0.96	≈1.00
Others	1–2	1/120–1/12		
	$h_1 = 1/6$			
0.1	1–2	1/72–1/6	0.93–0.98	
Others	1–2	1/120–1/12		
$h_1 = 1/8$				
0.1 and others	1–2	1/120–1/12	0.97–1.00	
$h_1 = 1/8$				
0.1 and others	1–2	1/120–1/12	≈1.00	

Note: others—$t_1/b = 0.05$, 0.025 and 0.01.

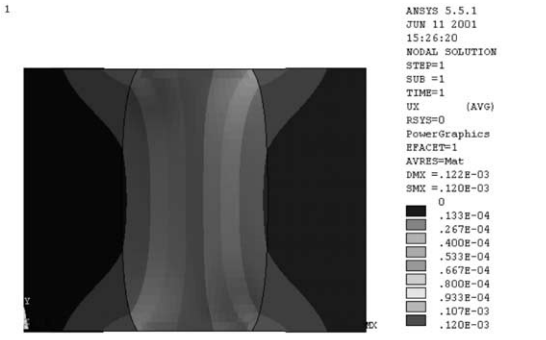

(a) UX (front view $+z$)

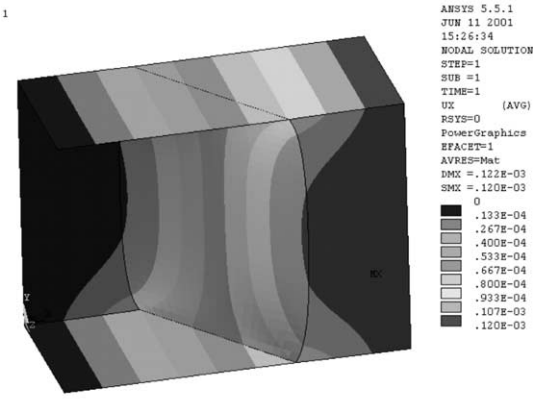

(b) UX (iso-view)

Fig. 18. Pure tension mode.

6. Summary and concluding remarks

In this paper, constitutive modeling of honeycomb sandwiches is developed, and an effective theoretical approach is proposed to derive elastic stiffness tensors for general honeycomb sandwiches. The usually neglected skin effect is given particular attention and is found playing an important role in both sandwich local fields and global behaviors.

First, the adaptation of homogenization theory to periodic plates is introduced and extended to include transverse shear deformation theory, by which the field equations of three local problems are deduced. Then a MPH technique is applied to solve the 3-D homogenization functions. With the first pass of the GTM, the spatial heterogeneity is conveniently transformed into the material anisotropy. In the second pass, the unit cell is 2-D homogenized by global plane strain, where the solution is analytically sought in a variational sense. The stiffness tensors are finally formulated in the form of Fourier series that is easily calculated with a symbolic program. Finally a FEA is conducted to verify and complement the analytical solutions with the additional assessment on the effect of skin rigidity.

In this study, there are several observations to be concluded as follows:

1. The MPH technique is successfully applied in periodic cellular structures, and the engineering application of the technique is thought prospective for structural homogenization. Further with the GTM, the

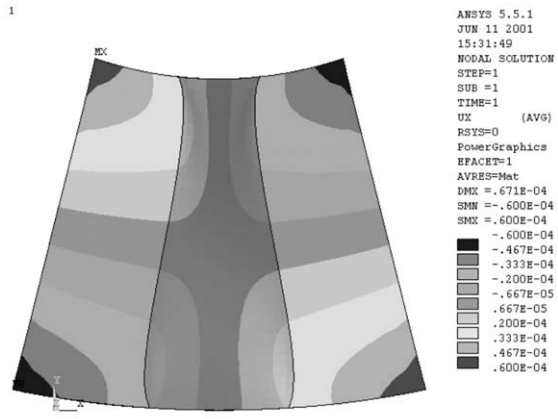

(a) *UX* (front view $+z$)

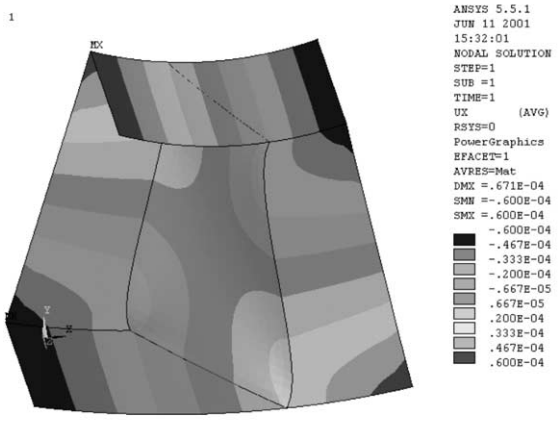

(b) *UX* (iso-view)

Fig. 19. Pure bending mode.

3-D anisotropic elasticity is practiced by the authors on real engineering problems, among very few cases in the literature. Honeycomb constitutive modeling, after incorporating these concepts, thus has much more flexibility in the improvement of computational accuracy and expense. It should be noted that the approach developed in this paper is readily applicable for all general 2-D cellular configurations and corrugated cores.

2. The adaptation of homogenization theory in periodic plates is introduced and modified by the authors to include transverse shear deformable plate theory. The homogenization function of transverse shear stiffness is for the first time derived with analytical solution, and along with other stiffness, transverse shear stiffness is validated with FEA and literature results. It is advised that for general computations the accurate calculations of stiffness follow the formulas (46), (61), (68), (77), (82) derived in this study complemented with the FEA-based equations (91) and (92) and the correction coefficients in Table 7. And a refined analysis may choose unit cell FEA with specialized code or periodicity modeling technique which is developed in this paper.
3. The flexural stiffness and stretch stiffness are for the first time distinguished from each other for honeycomb sandwich structures, by considering their symmetric and anti-symmetric responses. Although the

impact of this study on sandwich computational modeling needs further evaluations, the careful use of equivalent core properties is hereby emphasized, which include the sensitivity of Poisson's ratios.

4. The skin effect plays an important role in all sandwich stiffness for general practical honeycomb sandwiches, particularly when the thickness ratio ε/δ is not small. As today's sandwich computations never take it into account, there is a strong recommendation to include this effect in refined analysis and to have further investigations on practical applications. The particular one is of sandwich beams, on which many tests and investigations are based.
5. Non-linear effect is briefly assessed in this study, and is found negligible in the elastic range. However, a thorough study is required for more understanding on non-linear behavior and coupling among shear, stretch, and bending modes. Also the assessment of size and edge effects in cellular modeling can be a relevant topic, especially for the justification of divergence between theoretic and experimental results.

7. Further study

In this study, the eight elastic tensors of flexural, stretch, and transverse shear of orthotropic honeycomb sandwich plates have been derived. To complement the present study, the further research on the solutions of torsional (warping flexural) and in-plane shear stiffness is provided in Qiao and Xu (2002), and a complete set of stiffness components is therefore available for computational models of orthotropic sandwich plates.

Acknowledgements

Financial support for this study was received from the National Science Foundation—Partnerships For Innovation Program (NSF-PFI: EHR-0090472), the College of Engineering and Faculty Research Committee of The University of Akron. We appreciate the support and encouragement of Dr. S. Graham Kelly, Dean of Engineering at the University of Akron.

References

Adams, R.D., Maheri, M.R., 1993. The dynamic shear properties of structural honeycomb materials. Compos. Sci. Technol. 47, 15–23.

Allen, H.G., 1969. Analysis and Design of Structural Sandwich Panels. Pergamon Press, Oxford.

Astley, R.J., Harrington, J.J., Stol, K.A., 1997. Mechanical modeling of wood microstructure, an engineering approach. IPENZ Trans. EMCH 24 (1), 21–29.

Becker, W., 1998. The inplane stiffness of a honeycomb core including the thickness effect. Arch. Appl. Mech. 68, 334–341.

Bourgeois, S., Cartraud, P., Debordes, O., 1998. Homogenization of periodic sandwiches. In: Mechanics of Sandwich Structures. Kluwer Academic Publishers, Dordrecht, pp. 139–146.

Burton, W.S., Noor, A.K., 1997. Assessment of continuum models for sandwich panel honeycomb cores. Comput. Meth. Appl. Mech. Eng. 145 (3–4), 341–360.

Caillerie, D., 1984. Thin elastic and periodic plates. Math. Mech. Appl. Sci. 6, 159–191.

Chamis, C.C., Aiello, R.A., Murthy, L.N., 1988. Fiber composite sandwich thermostructural behavior: computational simulation. J. Compos. Technol. Res. ASME 10 (3), 93–99.

Cunningham, P.R., White, R.G., 2001. A new measurement technique for the estimation of core shear strain in closed sandwich structures. Compos. Struct. 51, 319–334.

Daniel, M.I., Abot, L.J., 2000. Fabrication, testing and analysis of composite sandwich beams. Compos. Sci. Technol. 60, 2455–2463.

Duvaut, G., 1977. Comportement macroscopique d'une plaque oerforee periodiquement, Lecture Notes in Math., vol. 594. Springer, Berlin, pp. 131–145.

Fortes, M.A., Ashby, M.F., 1999. The effect of non-uniformity on the in-plane modulus of honeycombs. Acta Mater. 47 (12), 3469–3473.

Gibson, L.J., Ashby, M.F., 1988. Cellular Solids: Structure and Properties. Pergamon, Oxford.
Grediac, M., 1993. A finite element study of the transverse shear in honeycomb cores. Int. J. Solids Struct. 30 (13), 1777–1788.
Hohe, J., Becker, W., 2001. A refined analysis of the effective elasticity tensors for general cellular sandwich cores. Int. J. Solids Struct. 38, 3689–3717.
Kelsey, S., Gellatly, R.A., Clark, B.W., 1958. The shear modulus of foil honeycomb cores. Aircraft Eng. 30, 294–302.
Lekhnitskii, S.G., 1968. Anisotropic Plates. Gordon and Breach Science Publishers, London.
Lewinski, T., 1991. Effective models of composite periodic plates—I. Asymptotic solution. II. Simplifications due to symmetries. III. Two-dimensional approaches. Int. J. Solids Struct. 27, 1155–1203.
Masters, I.G., Evans, K.E., 1996. Models for the elastic deformation of honeycombs. Compos. Struct. 35, 403–422.
Meraghni, F., Desrumanx, F., Benzeggagh, M.L., 1999. Mechanical behavior of cellular core for structural sandwich panels. Composites: Part A 30 (6), 767–779.
Noor, A.K., Burton, W.S., Bert, C.W., 1996. Computational models for sandwich panels and shells. Appl. Mech. Rev. ASME 49 (3), 155–199.
Parton, V.Z., Kudryavtsev, B.A., 1993. Engineering Mechanics of Composite Structures. CRC Press, Boca Raton, FL.
Penzien, J., Didriksson, T., 1964. Effective shear modulus of honeycomb cellular structure. AIAA J. 2 (3), 531–535.
Plantema, F., 1966. Sandwich Construction. John Wiley & Sons, New York.
Qiao, P.Z., Xu, X.F., 2002. Refined analysis of torsion of composite honeycomb sandwich structures. J. Eng. Mech. ASCE. (under review).
Shi, G., Tong, P., 1995a. Equivalent transverse shear stiffness of honeycomb cores. Int. J. Solids Struct. 32 (10), 1383–1393.
Shi, G., Tong, P., 1995b. The derivation of equivalent constitutive equations of honeycomb structures by a two scale method. Comput. Mech. 15, 395–407.
Takano, N., Zako, M., Kikuchi, N., 1995. Stress analysis of sandwich plate by the homogenization method. Mater. Sci. Res. Int. 1 (2), 82–88.
Vonach, W.K., Rammerstorfer, F.G., 1998. Effects of in-plane stiffness on the wrinkling load of sandwich constructions, Sandwich Constructions IV, vol. 1. EMAK UK.
Vougiouka, G., Guedes, H.R., 1998. Prediction of elastic properties of sandwich panels using a homogenization computational model. In: Mechanics of Sandwich Structures. Kluwer Academic Publishers, Dordrecht, pp. 147–154.
Warren, W.E., Kraynik, A.M., 1987. Foam mechanics: the linear elastic response of two-dimensional spatially periodic cellular materials. Mech. Mater. 6, 27–37.
Xu, X.F., 2001. On the Elastic Homogenization of Honeycomb Sandwich Structures. Master of Science Thesis, The University of Akron, Akron, Ohio.
Xu, X.F., Qiao, P.Z., Davalos, J.F., 2001. On the transverse shear stiffness of composite honeycomb core with general configuration. J. Eng. Mech. ASCE 127 (11), 1144–1151.
Zenkert, D., 1995. An Introduction to Sandwich Construction. Chamelon Press, London.